AFRL-AFOSR-VA-TR-2016-0337

Self-Diagnostic Adhesive for Bonded Joints in Aircraft Structures

Fu-Kuo Chang
LELAND STANFORD JUNIOR UNIV CA

10/04/2016
Final Report

Air Force Research Laboratory
AF Office Of Scientific Research (AFOSR)/ RTB2
Arlington, Virginia 22203
Air Force Materiel Command

REPORT DOCUMENTATION PAGE

Form Approved
OMB No. 0704-0188

1. REPORT DATE *(DD-MM-YYYY)*	2. REPORT TYPE	3. DATES COVERED *(From - To)*
27-10-2016	Final Performance	15 Mar 2013 to 14 Mar 2016

4. TITLE AND SUBTITLE
Self-Diagnostic Adhesive for Bonded Joints in Aircraft Structures

5a. CONTRACT NUMBER

5b. GRANT NUMBER
FA9550-13-1-0139

5c. PROGRAM ELEMENT NUMBER
61102F

6. AUTHOR(S)
Fu-Kuo Chang

5d. PROJECT NUMBER

5e. TASK NUMBER

5f. WORK UNIT NUMBER

7. PERFORMING ORGANIZATION NAME(S) AND ADDRESS(ES)
LELAND STANFORD JUNIOR UNIV CA
450 SERRA MALL
STANFORD, CA 94305-2004 US

8. PERFORMING ORGANIZATION REPORT NUMBER

9. SPONSORING/MONITORING AGENCY NAME(S) AND ADDRESS(ES)
AF Office of Scientific Research
875 N. Randolph St. Room 3112
Arlington, VA 22203

10. SPONSOR/MONITOR'S ACRONYM(S)
AFRL/AFOSR RTB2

11. SPONSOR/MONITOR'S REPORT NUMBER(S)
AFRL-AFOSR-VA-TR-2016-0337

12. DISTRIBUTION/AVAILABILITY STATEMENT
A DISTRIBUTION UNLIMITED: PB Public Release

13. SUPPLEMENTARY NOTES

14. ABSTRACT
Bondline integrity is one of the most critical concerns in the design and operation of aircraft and spacecraft structures up to date. Nevertheless, current state-of-the-art non-destructive evaluation (NDE) and structural health monitoring (SHM) techniques are incapable of offering mature solutions regarding bondline integrity monitoring. Therefore, the objective of the proposed research is the development of a complete approach for integrity monitoring and self-diagnosis of adhesively bonded structures. During the reporting period, three major accomplishments were achieved:
1) Screen-printed piezo-electric sensors of the new design were developed and fabricated. The new sensors had a smaller dimension compared to the previous design to minimize the parasitic effect when embedded into bondlines. 2) The developed impedance-based diagnostic algorithms were validated under the fatigue/dynamic loading condition. 3) Both SEM (Spectral Element Modeling) and FEM (Finite Element Modeling) simulation of the impedance of the embedded piezo-elelctric sensor was conducted.

15. SUBJECT TERMS
Bondline Integrity, Self-diagnosis, Nano/micro Sensors, Smart Adhesive

16. SECURITY CLASSIFICATION OF:			17. LIMITATION OF ABSTRACT	18. NUMBER OF PAGES	19a. NAME OF RESPONSIBLE PERSON
a. REPORT	b. ABSTRACT	c. THIS PAGE			LEE, BYUNG
Unclassified	Unclassified	Unclassified	UU		

Standard Form 298 (Rev. 8/98)
Prescribed by ANSI Std. Z39.18

				19b. TELEPHONE NUMBER *(Include area code)* 703-696-8483

Self-Diagnostic Adhesive for Bonded Joints in Aircraft Structures

Award Number FA9550-13-1-0139

Final Report

Reporting Period: March 15 2013 to March 14 2016

PI: Fu-Kuo Chang
Stanford University

Program Manager: B. L. ("Les") Lee

June 14, 2016

Table of Contents

Executive Summary 3
1.1 OBJECTIVES 4
1.2 TECHNICAL ACCOMPLISHMENTS 5
Development of a Novel Computational Algorithm for the Simulation of Diagnostic Wave Propagation in Adhesively Bonded Structures 5
Diagnostic Algorithms for Bondline Integrity Monitoring 10
Estimate the Strength of the Bondline via the Impedance of Embedded Piezoelectric Sensors 19
Improved Detectability with Multiple Sensors 22
Parametric Study of Sensor Performance via Finite Element Simulation 24
Screen-printed Micro-scale Piezo-ceramics onto Polymeric Films 30
Release of Screen Printed Piezo-ceramics onto a Polyimide Substrate 35
1.3 PUBLICATIONS 40
1.4 REFERENCES 41

Executive Summary

Bondline integrity is one of the most critical concerns in the design and operation of aircraft and spacecraft structures up to date. Nevertheless, current state-of-the-art non-destructive evaluation (NDE) and structural health monitoring (SHM) techniques are incapable of offering mature solutions regarding bondline integrity monitoring. Therefore, the objective of the proposed research is the development of a complete approach for integrity monitoring and self-diagnosis of adhesively bonded structures. The implementation will be based on the development of "intelligent" stretchable micro/nano-sensor networks that may be embedded inside the adhesive layer leaving a minimal footprint on the material. Special emphasis will be given to the detection of "kissing" bonds, which constitute a major challenge in the aeronautical and aerospace communities.

The proposed research involves:

a) Development of new types of micro/nano-sensors and actuators integrated into adhesive films without causing any degradation.
b) Development of computational and analytical algorithms for the numerical simulation of ultrasonic wave propagation and electromechanical impedance spectrum.
c) Novel self-diagnostic algorithms for monitoring the adhesive bondline integrity based on advanced signal processing and machine learning techniques.
d) Integration into a prototype adhesively bonded structure and assessment under various operating/environmental conditions.

The proposed technology will lead to the development of an "intelligent" adhesive able to monitor the bondline integrity, self-diagnose and indicate integrity degradation, and achieve the early detection of kissing bonds. This would lead to a paradigm change in the aircraft structure design by providing increased confidence and allowing for the use of bonded joints instead of bolted joints. The main advantages of bonded joints include the significant reduction of weight, which may reach up to 50% compared to bolted joints, the great economic impact resulting from the reduced assembly cost and the increased fuel efficiency, and the improved aircraft performance.

1.1 INTRODUCTION

Bondline integrity monitoring is still one of the most critical concerns in the design of aircraft and spacecraft structures up to date. Although adhesively bonded joints have demonstrated superior properties over mechanically fastened joints, current standards still require fasteners even with adhesive because of a lack of confidence on the integrity of the bondline in fabrication and during service. This reduces the benefits of bonding. There are two major types of defects in bondlines, gross defects and adhesive defects [1]. Debonds between adhesive/adherend and delaminations on substrates, which fit into first category, can be detected via NDE methods like C-scan or ultrasonic reflection [2-5]. Those methods have been proven to be effective to a certain extent. However, specimen preparation takes a long time in all of these methods. Recent work in structural health monitoring, by Ihn and Chang [6-8], has demonstrated the ability to identify debonds in real-time, using built-in piezoelectric discs to generate ultrasonic waves.

An adhesive defect is seen as traction-free contacted surfaces, which show reduced bond strength and are difficult or impossible to detect using conventional NDE [5]. Kissing bonds are one of the major adhesive defects and possess little residual tensile or shear strength. Many factors may lead to kissing bonds, including surface contaminates, adhesive chemistry, inappropriate curing stress, residual stress, moisture ingress, etc. As a result, kissing bonds can appear in a local fashion and the only way to detect them is to measure the local adhesive during fabrication and in service to track its degradation [5, 9-17]. Kissing bonds are the most critical and challenging defect to be detected in bonded joints and significantly influence the confidence of bondline integrity after the joints are placed in service.

Embedding micro/nano sensors inside the adhesive layer has the potential to be an effective solution to this challenge. Upon initial inspection, this approach may not seem feasible because adding new materials inside adhesive will increase the risk of contamination and introduce new defects. However, industry has begun to use adhesive films with fiber scrims inside, to ease handling and improve quality control. For example, Henkel embeds nylon scrim material into Hysol EA9696 film adhesives. This indicates that this approach is feasible if shrinking the sensors down to the size of typical fibers and making them out of the same materials as current scrims so that the adhesive will have the same mechanical performance as well as the capability to monitor its own integrity degradation level can meet the standards.

1.2 OBJECTIVES

Develop integrated hardware and diagnostic algorithms built on the expandable network substrate to enable state sensing and bondline integrity monitoring. This system is intended to incorporate multiple forms of sensors in a micro-fabricated network. The outputs of this network need to be interpreted to provide useful information for bondline integrity monitoring.

More specifically, the objectives of the project are:

a) Development of active and passive micro/nano sensors and actuators.

b) Development of highly stretchable sensor networks. These sensor networks shall be embedded inside the adhesive and will cover a large area of the bondline with minimal footprint on the structure.
c) Development of computational algorithms and analytical models for the numerical simulation of the diagnostic Lamb wave propagation and the modeling of the electromechanical impedance (EMI) spectrum as measured at the sensor terminals.
d) Development of diagnostic algorithms for the assessment of the adhesive bondline integrity. These algorithms will be based on a combination of the aforementioned computational and analytical models along with advanced signal processing techniques in order to optimally treat the acquired sensor signals and interpret the bondline interface integrity.
e) Integration of the developed stretchable sensor network into an adhesively bonded joint and subsequent characterization of the bondline integrity using data obtained under various operating conditions and the developed diagnostic algorithms.

1.3 TECHNICAL ACCOMPLISHMENTS

The stretchable network technology developed at Stanford University provides a starting point and substrate on which to build a network consisting of sensors, electrical interconnects. This network will be employed for the development of a smart adhesive film with self-diagnosis capability.

Work and accomplishments in this pursuit include:

1) Development of release approach of screen-printed piezo-ceramics onto a polyimide substrate.
2) Development of a numerical tool for the numerical simulation of the diagnostic Lamb wave propagation and the modeling of the electromechanical impedance (EMI) spectrum as measured at the sensor terminals
3) Development diagnostic algorithms for the assessment of the adhesive bondline integrity.

Development of a Novel Computational Algorithm for the Simulation of Diagnostic Wave Propagation in Adhesively Bonded Structures

Problem Statement

An efficient and accurate computation algorithm for the numerical simulation of the propagation of diagnostic waves in adhesively bonded structures needs to be developed. This algorithm will be employed in order to characterize the behavior of the self-diagnostic adhesive with the embedded sensor network, as well as it will also contribute to the optimization of the design of the sensor network itself. Previous relevant work, multi-physics simulations by spectral element methods, has been carried out and proved to be effective in modeling cracks and delaminations as well as varying environmental and operating condition, such as temperature and loading effects on sensor signals

Method of Approach

In order to enable a reliable simulation of the diagnostic wave propagation in adhesively bonded joints and structures, a novel computational algorithm was developed for the special needs of the proposed research. Once appropriately calibrated, the algorithm was able support a model-assisted bondline monitoring approach by providing diagnostic data for a large range of environments. Hence, the model needs to capture how the SHM system is affected by environmental and operational uncertainties, such as temperature, ambient loads etc.

An in-house computational code based on time-domain Spectral Element Methods (SEM) has been developed in order to simulate electro-mechanical problems like ultrasonic wave propagation in smart structures induced by surface mounted piezoelectric transducers Figure 1. The developed Piezo Enabled Spectral Element Analysis (PESEA) code is capable of modeling basic environmental effects, such as temperature variations, which significantly affect the diagnostic wave propagation in structures. To ensure a highly efficient computation, an explicit time integration scheme is adopted, while SEM can efficiently model piezoelectric materials as well as adhesive layers as thin as 10-20 μm.

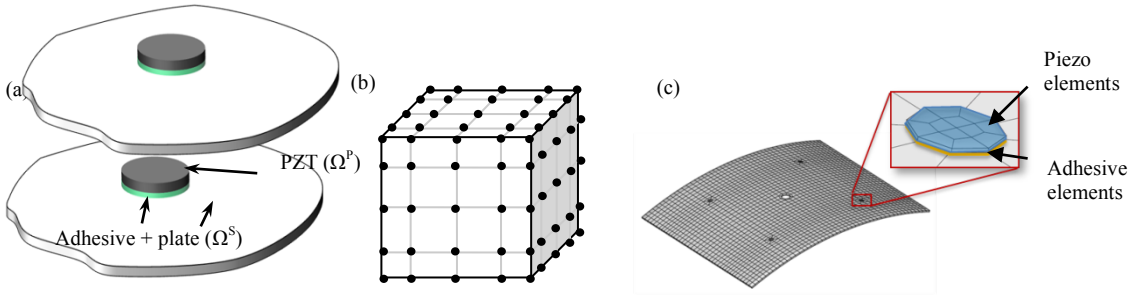

Figure 1: (a) Embedded piezoelectric sensor, (b) solid spectral element of order 4×4×4, and (c) modeling of piezoelectric transducers and adhesive layers.

Results

A numerical study was conducted on the embedded piezo sensor inside lap joints. The frequency range that we are interested is around 800 kHz. Conventional linear finite element method (FEM) requires a very fine spatial discretization in order to handle the high-frequency nature of these situations, which results in high computational cost. The dimension and the meshes of the model are illustrated in Figure 2, Table 1 – Table 3. The center region has a finer spatial discretization in order to capture complicated electro-mechanical behavior of embedded piezo sensor. Sinusoid signals of 50 volts amplitude with various frequencies were exerted on the top and bottom surface of the piezo disc sensor. The mechanical deformation of the sensor is calculated as well as the electrical charge. The ratio and phase difference between input voltage and output charge provide the real and imaginary impedance as illustrated in Figure 3.

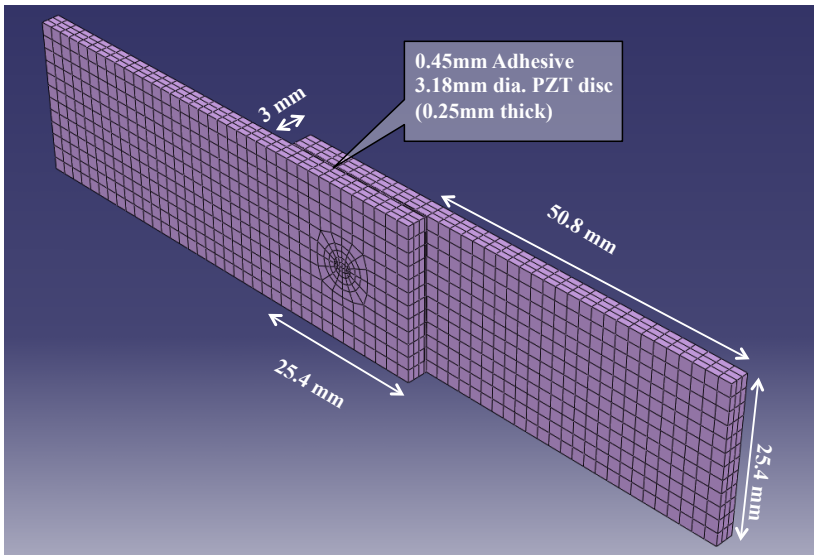

Figure 2: The dimension and the mesh of the lap joint model for the SEM numerical simulation.

In order to simulate the damage due to the cyclic loads, the cracks were simulated by artificially decrease the tensile and shear modulus of the adhesive layer between aluminum adherent and piezo sensor to 0.1% of its original value. We investigated the impedance as well as damage index (RMSD from 600 kHz to 700 kHz) under different size of damage are. Even though the nature of kissing bond is still unknown, the simulation using cracks would provide an initial insight on how the sensors behave under damaged situation.

Table 1: The SEM mesh details.

Total Element No.	Aluminum laps	Adhesive layer	Piezo Sensor
4890	4278	584	28

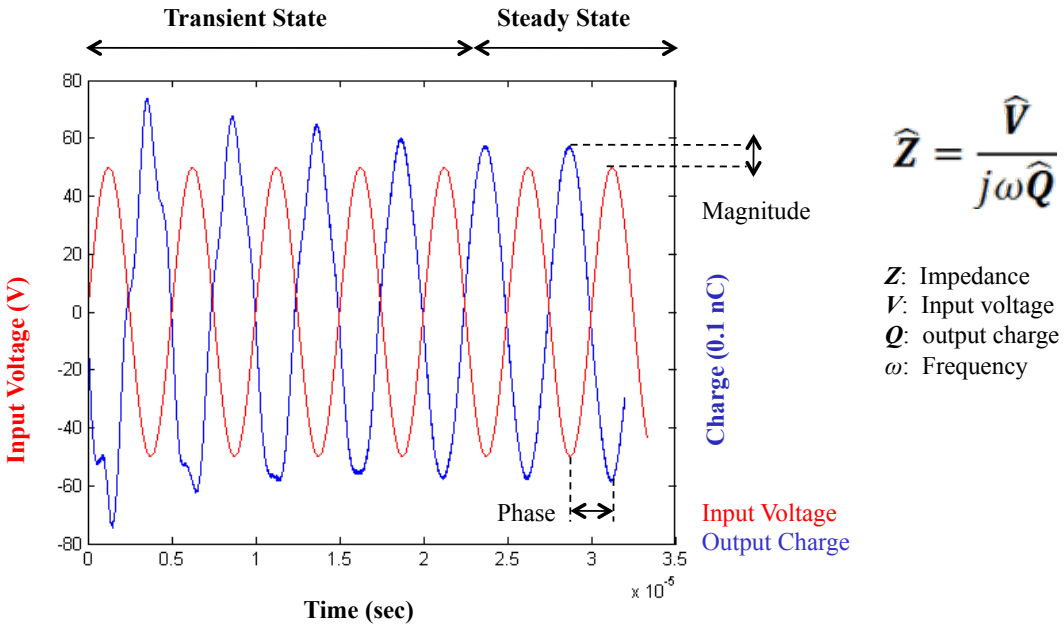

Figure 3: The ratio and phase difference between input voltage (red) and output charge (blue) determine the electromechanical impedance.

Table 2: The mechanical properties used in the SEM numerical simulation.

Property	Unit	Al 2024-T3	Adhesive Hysol EA 9696	Piezo PZT-5A
E11	GPa	69	2.6	60.97
E22	GPa	69	2.6	60.97
E33	GPa	69	2.6	53.19
G23	GPa	25.94	1	21.05
G12	GPa	25.94	1	22.57
G31	GPa	25.94	1	21.05
ν23		0.33	0.3	0.4402
ν12		0.33	0.3	0.35
ν13		0.33	0.3	0.4402
ρ	kg m−3	2700	1100	7750

Table 3: The electromechanical and electrical properties of the piezo material used in the simulation.

$$\mathbf{d} = \begin{bmatrix} 0 & 0 & 0 & 0 & 584 & 0 \\ 0 & 0 & 0 & 584 & 0 & 0 \\ -171 & -171 & 374 & 0 & 0 & 0 \end{bmatrix} \times 10^{-12}\,\mathrm{C\,N^{-1}}$$

$$\varepsilon_\sigma = \begin{bmatrix} 1730 & 0 & 0 \\ 0 & 1730 & 0 \\ 0 & 0 & 1700 \end{bmatrix} \times \varepsilon_0$$

Figure 4 illustrates the various size of damage region from 0% to 50%, which half of the bondline was damaged. The corresponding damage index is plotted in Figure 5. With the increase of damage size, the damage index of simulated result showed similar behavior as the experimental result, i.e. the damage was relatively constant and the damage index increased significantly when the damage region approached the piezo sensor.

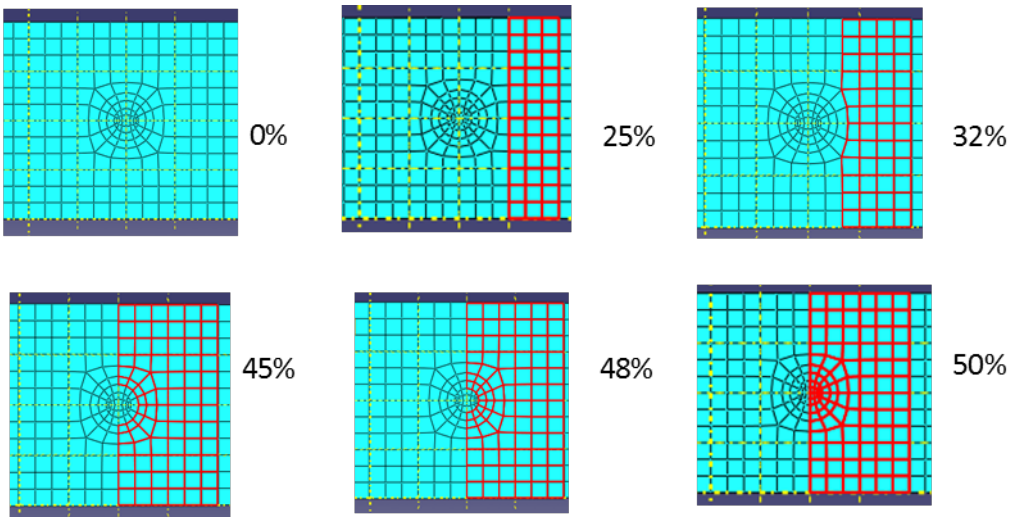

Figure 4: By decreasing the modulus of a certain adhesive region to 0.1% of its original value, the various levels of damage were simulated.

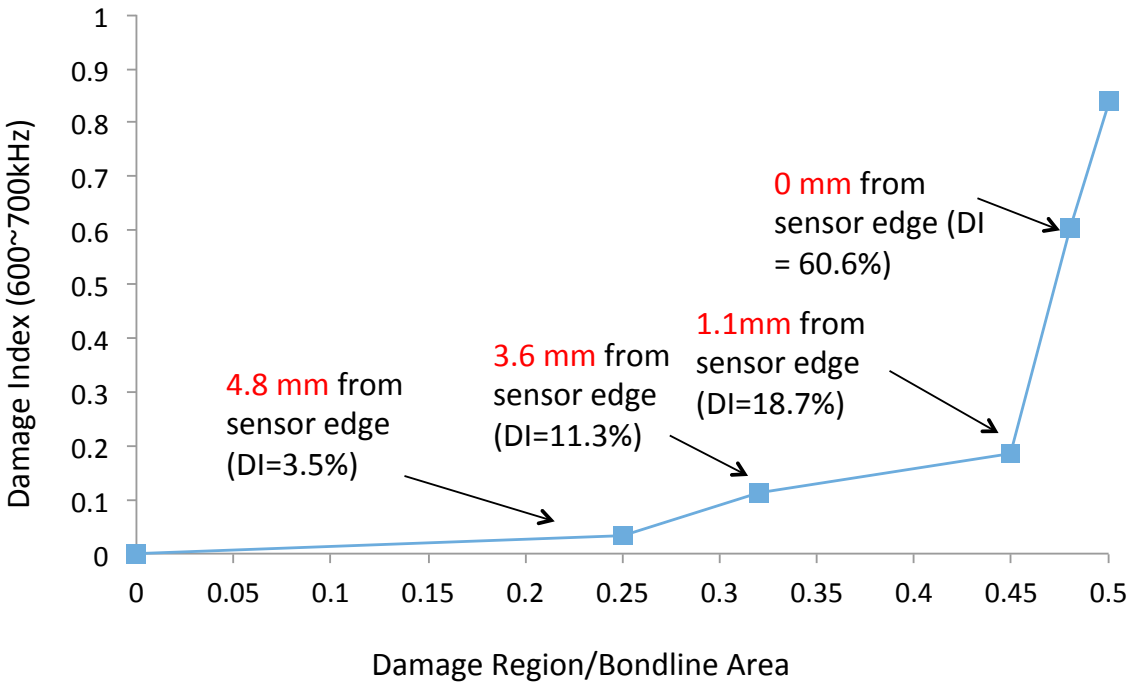

Figure 5: The damage index of the simulation-based results exhibit similar behavior with the experimental results and increase with the decrease of distance between front of damage region and sensor edge (shown in red).

Diagnostic Algorithms for Bondline Integrity Monitoring

Piezoelectric transducers are widely used for active sensing/interrogation of both near-field (local[1]) and far-field (remote) structural damage. Sensing of near-field defects or damages can be carried out by using high-frequency (>30 kHz) impedance-based methods that monitor changes in the structural stiffness, damping, and mass. Piezoelectric transducers acting in the "direct" manner produce an electrical charge when stressed mechanically. Conversely, a mechanical strain is produced when an electrical field is applied. The process to be used with impedance-based monitoring methods utilizes both the direct and converse versions of the piezoelectric effect simultaneously in order to obtain an impedance signature

Problem Statement

The goal of this task is to develop effective and robust diagnostic tools using impedance and ultrasonic wave based methods for near-field (local) and far-field (remote), respectively, adhesive bondline integrity monitoring and assessment using the embedded sensor network. Special emphasis shall be given to the early detection of kissing bonds, as currently there are neither mature methods nor techniques that provide an efficient solution to this extremely important issue.

Method of Approach

A schematic representation of the currently proposed diagnostic framework for bondline integrity monitoring and assessment is presented in Figure 6. The ultimate objective is to combine data driven techniques with the physics based strategies developed. Starting with coupon level tests in the laboratory, the sensor data were collected under varying operating conditions (varying load cycles). The sensor data was processed using advance signal processing techniques in order to extract appropriate damage sensitive features. These features will be used in a later stage by the machine-learning algorithm in order to classify the actual damage state of the structure.

Further, the identified damage state needs to be also quantified in order for this information to be used for the prognosis of the remaining useful life of the bondline integrity. However, under varying environmental and operating conditions the sensor data shall often be masking the effect of structural defects or damage. For this reason, the development of analytical or physics based models that can filter out and isolate the effect of damage in the sensor data is necessary. The models that are capable of compensating the effect of varying environmental and operating conditions on the sensor's response can be developed based on the physical insight using PESEA-based simulations. Compensated sensor data combined with machine learning algorithms can be then used for the accurate assessment of the bondline integrity, which will be later validated on typical adhesively bonded structural components.

[1] Local or remote with respect to the sensor location employed.

Results

Single lap joints with piezo sensors embedded were prepared to investigate the relationship between the electromechanical impedance behavior of the piezo and the load history on the lap joints (see Figure 7). The samples were prepared following the ASTM D1002 (Standard Test Method for Apparent Shear Strength of Single-Lap-Joint Adhesively Bonded Metal Specimens by Tension Loading (Metal-to-Metal)), with 1 inch by 1 inch of bondline area for one sensor embedded and 2 inch by 1 inch for two sensors embedded sample.

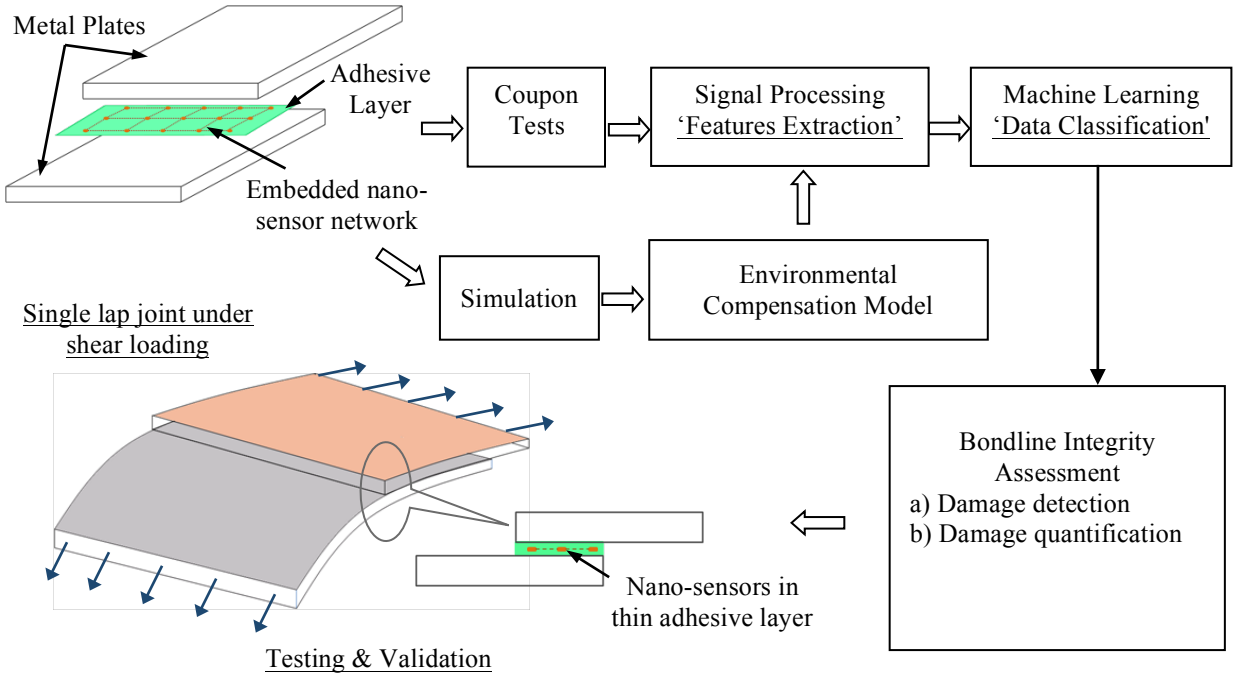

Figure 6: Schematic representation of the proposed framework for bondline integrity monitoring and assessment.

Hysol EA 9696 adhesive film provided by Henkel was used to bond two aluminum alloy laps (6061 T5). Hysol EA 9696 is a modified epoxy film designed for applications requiring high toughness including aeronautics. The surface of the aluminum laps was roughened using sandpaper. After that, high-pressure air and acetone were deployed to remove all the debris and grease. Following the instruction by the manufacturer, we cured the samples under vacuum for 90 minutes at 121°C.

In order to simulate the "kissing" bond behavior, different types of chemicals were used to degrade the bondline strength, including Teflon and graphite powder, two common materials found in manufacturing of carbon composite fibers. The result is shown in Figure 8. Graphite powder was used as the surface contaminates in the latter test due to its large influence on the bond strength and relative ease to handle.

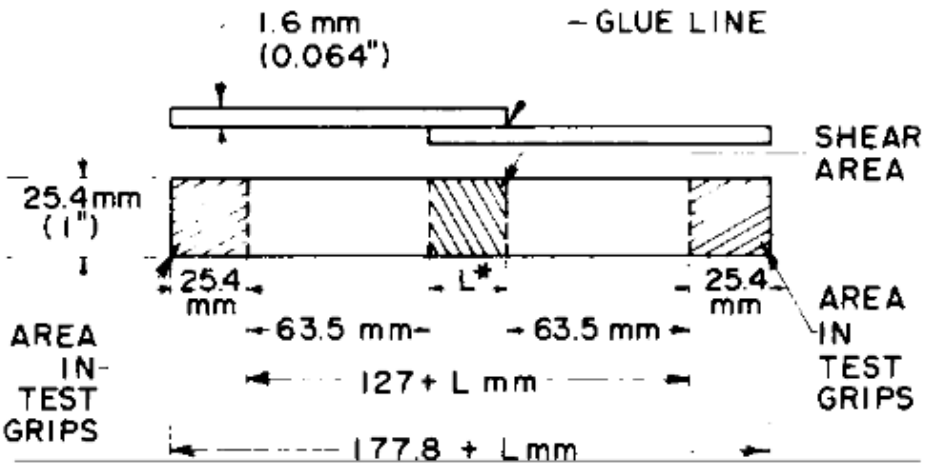

Figure 7: Suggested form and dimensions of test specimen in ASTM D1002

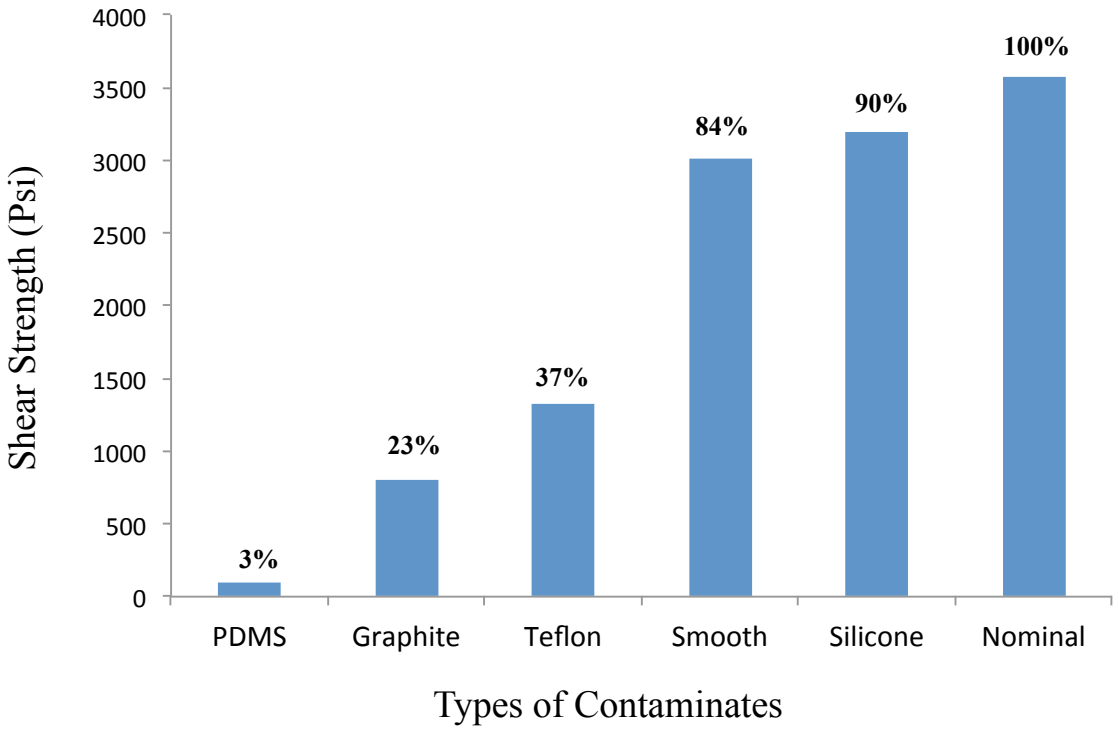

Figure 8: The influence of different surface contaminates on lap joint strength.

Piezoelectric disc sensors fabricated by APC ceramics were embedded into the bondline. The piezo material was Navy II type equivalent with 250 um in thickness and 1/8 inch in diameter. The material properties can be found in Table 4.

Table 4: The properties of the piezoelectric material in APC disc sensor.

Density	Young's Modulus E_{11}	Young's Modulus E_{33}	Relative Dielectric Constant K_T	Piezo Charge Constant d_{33}	Piezo Voltage Constant g_{33}
7.6 g/cm^3	63 GPa	54 GPa	1900	400 pC/N	24.8 mV-m/N

Due to the thickness of the piezoelectric disc sensors, four layers of adhesive film were used to fully encapsulate the sensors. Two varnished wires with diameter less than 100 um were also embedded to extend the two electrodes of sensor to the outside of bondline, which are connected impedance analyzer. The lay-up of the sample is illustrated in Fig 3.

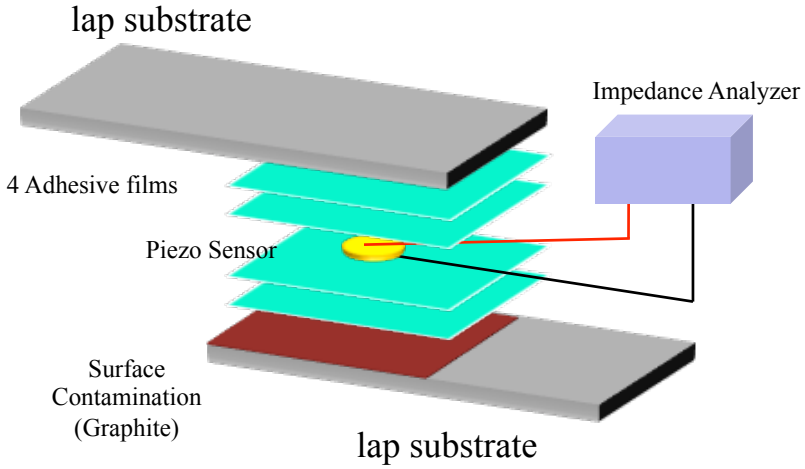

Figure 9: Illustration of a single lap joint with one piezoelectric sensor embedded in the adhesive bondline interface.

The sample was loaded on a MTS (Material Testing System) so that the introduced cyclic load can further degrade the bondline integrity. The overall setup is shown in Figure 10. The implemented cyclic load had an increasing peak load of 25 pounds step until sample failure and the impedance was measured under zero-load condition by Z-check 16777k impedance analyzer, a USB-powered impedance analyzer made by SinePhase. The impedance behavior of the piezo was recorded from 1kHz to 2.5MHz with an increment of 2kHz. Both the real and imaginary impedance data were acquired.

A total of 16 samples were tested. The cyclic load with an increment of peak value was exerted on the specimens. A typical load history curve will be similar as illustrated in Figure 11.

Table 5: A total of 16 specimens, 8 nominal samples without contaminate and 8 with contaminates, were tested.

	Nominal	Weak	Total
Batch 5	2	2	4
Batch 6	2	2	4
Batch 7	2	2	4
Batch 8	2	2	4
Total	8	8	16

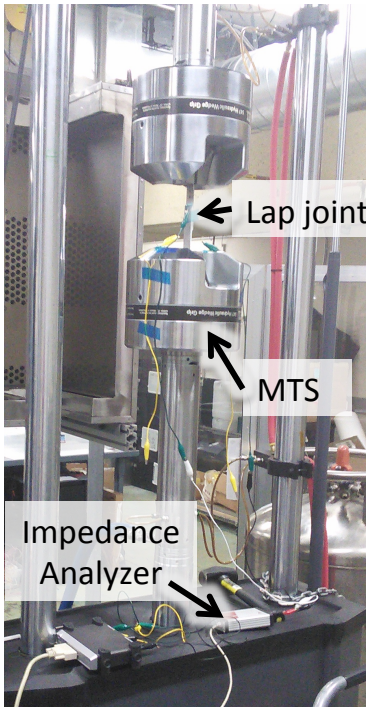

Figure 10: The experimental test setup.

After each load cycle, the electromechanical impedance was measured using the impedance analyzer. The typical impedance behavior will be similar to what is shown in Figure 12. There are two resonate peak of impedance shown in the measured frequency bandwidth between 500 kHz to 2.5 MHz. The first peak is recorded around 800kHz and the second peak with lower amplitude is found around 1.7 MHz. Similar impedance behavior was observed throughout all samples under all loading condition with slightly difference in frequency and amplitude.

We investigated several existing literature damage indices to evaluate the influence of the load cycle on the behavior of the piezoelectric sensors and the bondline integrity. We selected the root mean square deviation (RSMD) as the appropriate damage index, which described the averaged impedance change from the baseline or the sample without any loading. The definition of RMSD is shown below, where $Z_h(\omega_i)$ is the healthy bond's impedance, $Z_i(\omega_i)$ is the unknown or damaged bond's impedance and ω_i is the frequency interval.

$$RMSD = \sqrt{\frac{\sum_{i=1}^{N} [Re(Z_h(\omega_i)) - Re(Z_u(\omega_i))]^2}{\sum_{i=1}^{N} [Re(Z_h(\omega_i))]^2}}$$

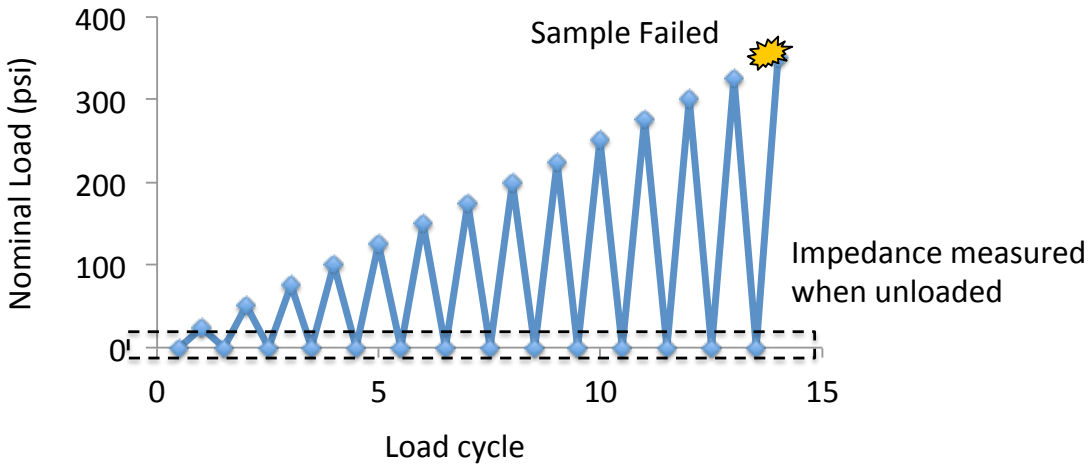

Figure 11: Typical load cycle with the impedance measured under the unloaded condit

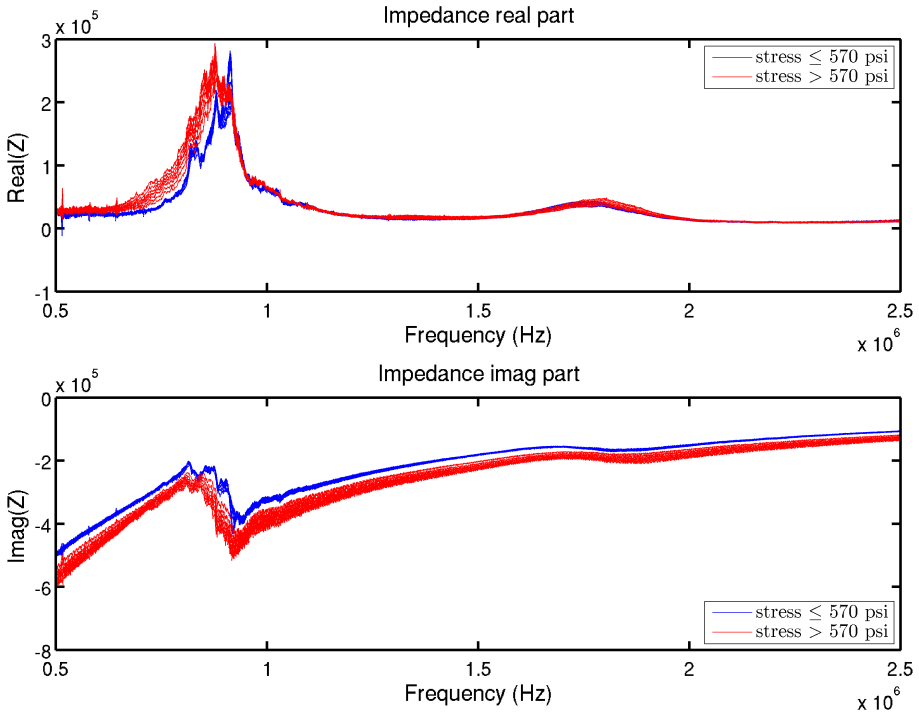

Figure 12: Typical electromechanical impedance behaviour obtained from experimental samples.

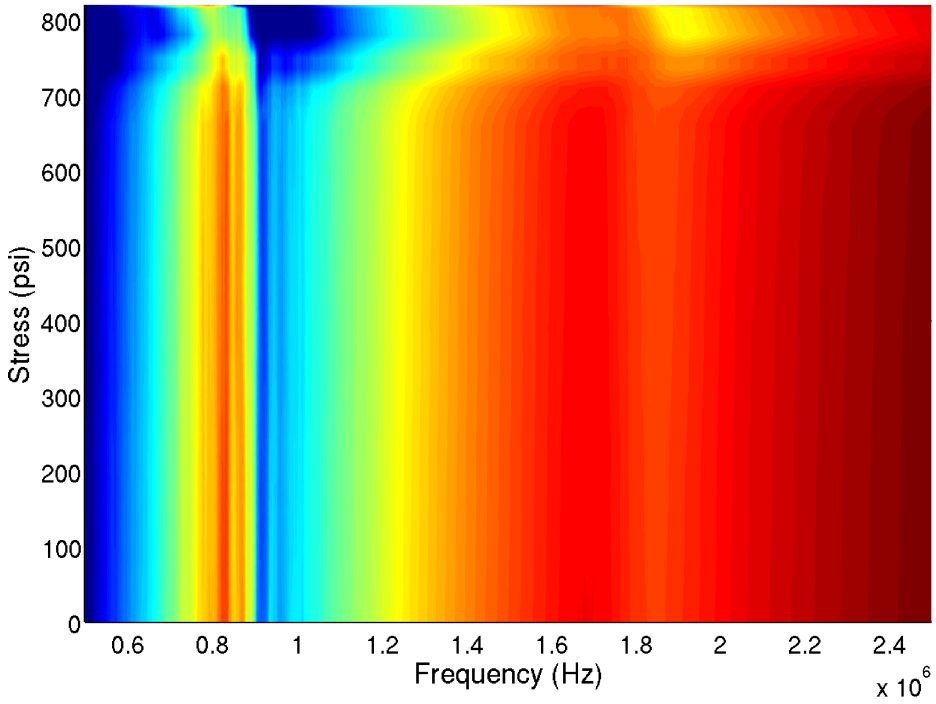

Figure 13: Indicative results of the imaginary part of the electromechanical impedance versus maximum load level under each cycle.

We estimated the damage index around the first peak frequency of 100 kHz frequency range. The damage index result is shown in fig. 3 in which the weak samples are specimens with surface contaminate.

Regardless of existence of surface contaminates, all samples showed a similar behavior, i.e. the damage index was relatively constant until the sample was exposed certain level of load cycle and approaching the failure. It implied that by measuring the impedance and the deviation of impedance from the intrinsic sample, it is possible to predict the failure of the bonded joint and estimate the degradation of bondline. For example, as shown in Figure 14, we chose the 2% damage index as an arbitrary threshold to separate the bondlines into healthy and degraded state.

In addition, a stochastic statistical model based method was also developed for bondline integrity monitoring and evaluation. These methods employ statistical model building on the time and/or frequency domains, baseline measured data under the nominal bond structural condition, and statistical decision making schemes for inferring the actual structural health state. Figure 15 presents a schematic representation of the statistical model based method for bondline integrity monitoring. The method utilizes the stochastic model parameters as the damage sensitive feature based on which a statistical characteristic quantity is constructed. At the final stage, a statistical decision making scheme is employed to determine the actual bondline health state.

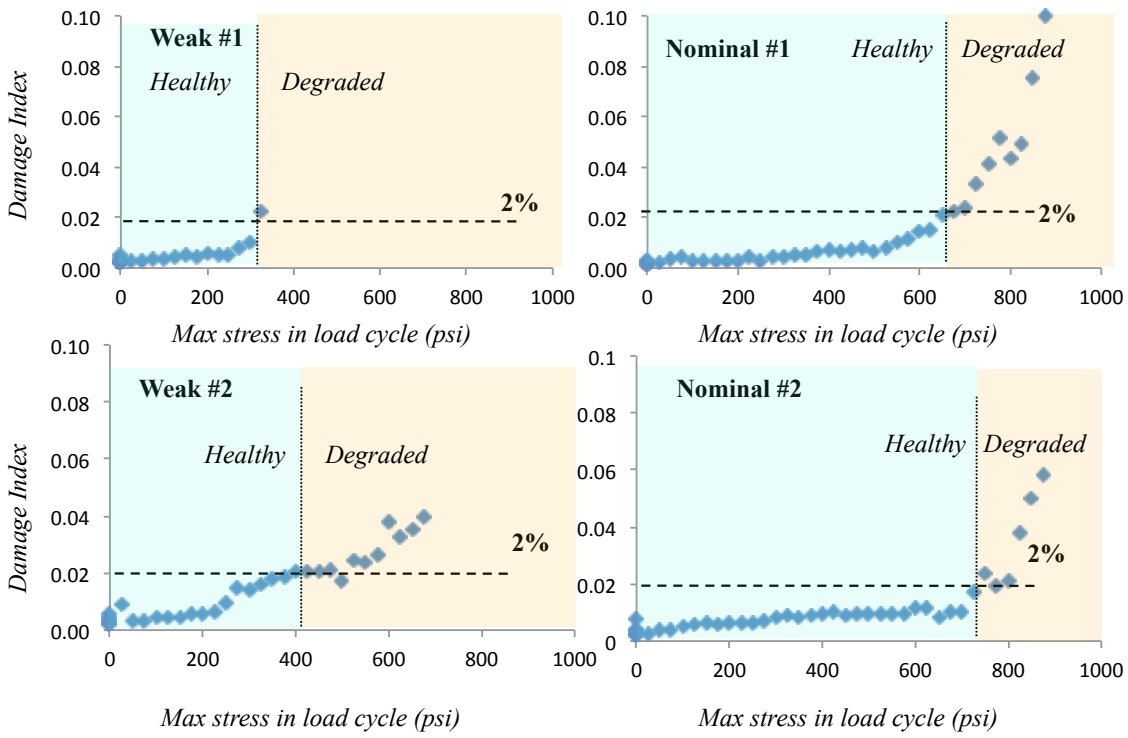

Figure 14: The damage index (root mean square deviation) of both weak and nominal samples exhibited a similar trend.

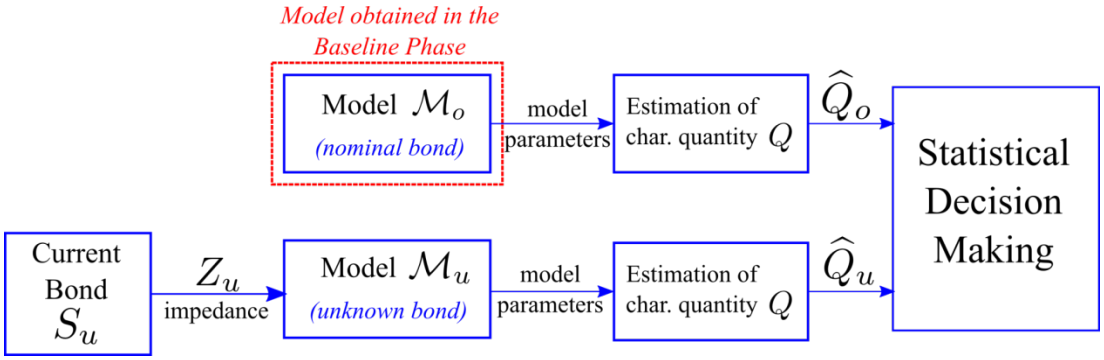

Figure 15: Schematic representation of the statistical model based method for bondline integrity monitoring.

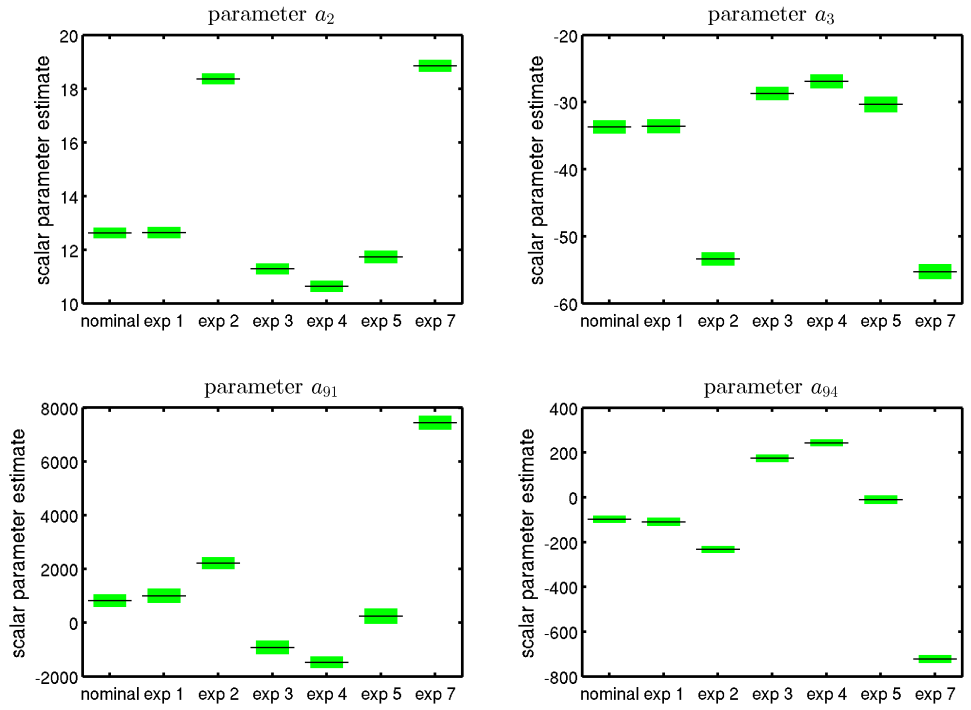

Figure 16: Indicative stochastic model parameters for various experiments corresponding to different maximum loading conditions for the same adhesively bonded joint. The scalar parameter estimates are depicted in black lines, while the 99% statistical confidence in

Figure 16 presents indicative stochastic model parameters for various experiments corresponding to different maximum loading conditions for the same adhesively bonded joint. The estimated parameters belong to a stochastic AutoRegressive with eXogenous input (ARX) model in the frequency domain. The model has been identified from baseline experiments under the nominal (healthy) adhesive bondline. In this figure, the scalar parameter estimates are depicted in black lines, while the 99% statistical confidence intervals are shown in green boxes. The main idea lies in the fact that the parameter estimates obtained under the current, "unknown" structural health state will overlap, as being statistically equal, with the nominal model's estimated parameters only if the current health state is the nominal one. Based on this fact, statistical multivariate damage indices may be constructed based on which the bondline integrity will be monitored and assessed.

Figure 17 presents indicative results for the prediction of the RMSD damage index (DI) using an adaptive Recursive AutoRegressive (RAR) time series model. The results indicative the predictive ability of the model, as well as the narrow confidence intervals of the predicted DI values. The figure presents the one-step-ahead prediction results, meaning that once we get the current value of the DI via experimental measurements we predict the future value of the DI. This technique may be improved and further developed to provide accurate precursors for the prediction of the bondline integrity of adhesively bonded structures.

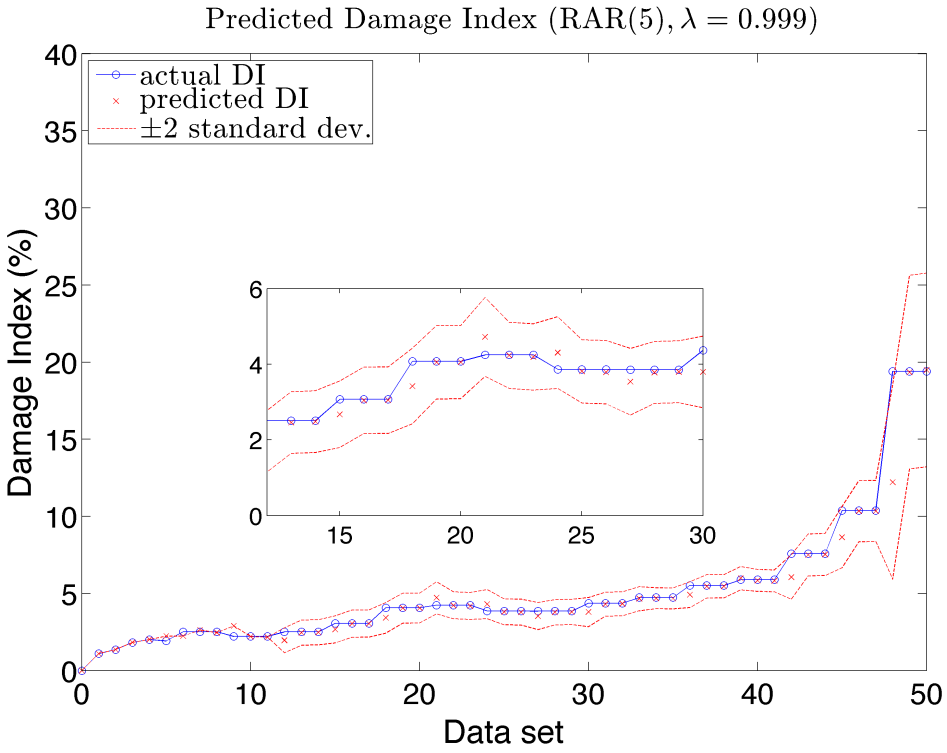

Figure 17: Damage index (DI) prognostics: actual DI versus predicted DI and 99% confidence intervals.

Estimate the Strength of the Bondline via the Impedance of Embedded Piezoelectric Sensors

From the previous section, the impedance of the embedded sensor in the bondline will start to deviate from the baseline data when the bondline is exposed to static loading. The deviation, also as defined as damage index will increase when the static loading across the bondline increases and the bondline starts to degrade. In this section, the model to predict the static strength of the bondline via the impedance of the embedded piezoelectric sensors based on previous experimental result is presented. The model is also verified via static shear test across unknown bonded single lap joints.

Problem Statement

The goal of this task is to estimate the static strength of unknown bondlines based on previous loading history and the impedance of the embedded piezoelectric sensor. The challenge of the method would be to predict the strength as early as possible with accuracy.

Method of Approach

Based on the impedance of samples tested before as well as the loading history, different models were developed in order to capture the correlation between the static loading history as well as the potential degradation to the bondline and the deviation of the impedance from the bondlines.

The results from previous test, a total of five samples, would be used to find a general model to describe the evolution of the impedance of the embedded sensor to the static loading. Once the model has been determined, two single lap joints with unknown strength due to insufficient surface preparation on purpose would be tested to validate the model as well as to predict the strength of the sample.

Results

In order to determine the proper model for predicting the static strength of a bondline sample, we chose the impedance result from five lap joint samples. The bondline area of all five samples and the sensor is positioned in the middle of the bondline. The sensors are fabricated by APC ceramics with a square shape of 2 mm width and the thickness of 0.2 mm. With the different level of the bondline surface preparation, the samples show a range of strength. The result of the strength is listed in the following table.

Sample Name	Strength (psi)
BB01	3200
B9K3S1	1225
B8N1	1100
B7N2	1000
B7N1	950

The sample BB01 showed the highest strength around 3200 psi and the failure mode is the cohesive failure, which indicated a good surface preparation. The rest of the samples showed the strength from 950 psi to 1225 psi and the adhesive failure were the dominant failure modes, which indicated an inefficient surface preparation and premature failure.

The data from five samples was then used to create the model to describe the general behavior between the external loading and the impedance deviation of the embedded sensor from its baseline of the pristine state. From the previous observation, the damage index and the normalized external load show a similar trend regardless of the strength of the sample. As a result, the normalized loads (the ratio between the external loads to the maximum load) are set as the inputs of the model and the damage index based on imaginary impedance is set as the output of the model.

Matlab R2013b is used to find the curve fit for the model and the two-term exponential model is chosen. The two-term exponential model has the following form as follows:

$$y=ae^{bx}+ce^{dx}$$

The result of the data, the two-term exponential model as well as the range with 50% confidence level is shown in Figure 18. In general, the constant a from the first term is greater than the constant c from the second term; while the coefficient c from the first term is less than the coefficient d from the second term. The first term is dominant for early stage and the second term is dominant for late stage. The coefficient result of the 50% confidence level is shown in Table 6.

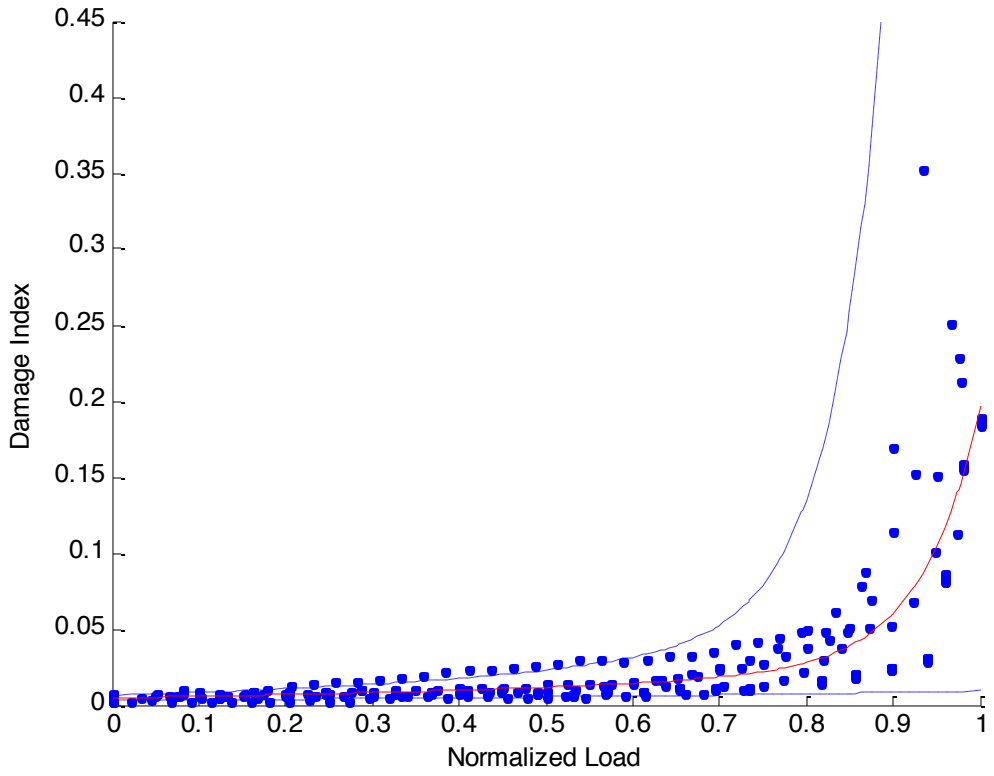

Figure 18. The two-term exponential model (solid line) of the 5 sets of the input data (dots) between the normalized load and the damage index based on imaginary impedance and its 50% confidence level (dashed lines)

Table 6. The value of the coefficient in the model.

constant	a	b	c	d
-50% confidence level	0.0030	1.12	-2.92e-08	13.56
Curve fit	0.0048	1.79	3.76e-08	15.31
+50% confidence level	0.0066	2.46	1.04e-07	17.05

In order to verify the model, another sample was prepared with the similar setting as previous samples. The similar static loading process was applied to the sample and the impedance was recorded at various loads. The load ratio between load and the strength was estimated based on the model and the predicted strength was derived as shown in Table 7.

Table 7. The measured load and impedance will provide a predicted strength using the model.

Measured Load(psi)	Damage Index	Predicted Load Ratio	Predicted Strength
500	0.005	0.045	11170
1000	0.006	0.129	7780
1500	0.008	0.311	4816
1700	0.012	0.503	3380

1800	0.014	0.575	3131
1900	0.017	0.669	2842
2000	0.020	0.724	2764
2100	0.024	0.771	2723
2200	0.030	0.810	2716
2300	0.038	0.846	2718
2400	0.049	0.877	2735
2500	0.061	0.902	2772
2600	0.087	0.935	2782
2700	0.169	0.989	2731

The correlation between the load exerted across the sample and the predicted strength is plotted in Figure 19. At the early stage where the external load is low, the predicted strength is much higher than the actual strength of 3000 psi due to the limitation of model. With the increase of the external load, the predicted strength start to converge and at around 60% of its full loading capability, the predicted strength keeps constant at around 2700 psi. The actual strength of the sample was slight less than 3000 psi and the model gave a conservative predicted strength of 2700 psi, around 10% less than the actual value. By tuning the model correspondingly, the prediction could be more conservation or less. This result indicates that it is possible to predict the strength of a bonded structure by the impedance of embedded piezoelectric sensor.

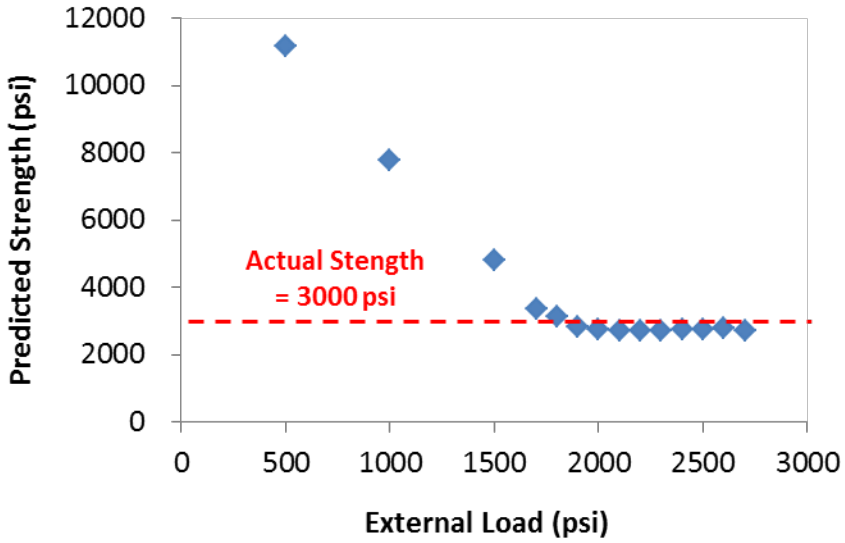

Figure 19. The prediction of the failure strength converges at 2700 psi with the sample exposed to more and more external load; the predicted value is 10% conservative than the actual 3000 psi strength.

Improved Detectability with Multiple Sensors

One of the challenges of using impedance-based algorithm for damage/degradation detection is that most techniques can only be applied to a relatively short distance [1]. Furthermore, the change of impedance can only occurred when the sample was approaching the failure under the current test setup and design of samples. Bondlines with multiple sensors embedded can address both issues.

Problem Statement

The task of this work is to embed multiple sensors into bondlines and to monitor the different response of the sensors after the same loading history. By positioning the sensor at various locations, we expect to see an improved detectability i.e. to monitor the failure of the bondlines earlier.

Method of Approach

The test setup is similar to the previous static loading test with single sensor. The single lap joint samples with commercial piezo-electric sensors embedded in the bondlines are prepared and exposed to fatigue loading. The samples are prepared following the ASTM standard D2651, *Standard Guide for Preparation of Metal Surfaces for Adhesive Bonding*, and the fatigue test is conducted following ASTM D1002, *Standard Test Method for Apparent Shear Strength of Single-Lap-joint Adhesively Bonded Metal Specimens by Tension Loading (Metal/Metal)*. The impedances of all sensors are recorded after certain static load until loaded to failure.

The finite element model is also to be developed to simulate the electro-mechanical behaviors of the embedded piezo-electric sensor in the bondlines. The direct steady-state linear dynamic analysis is chosen to estimate the behavior across a large range of frequency.

Results

A large bondline (2 inch by 1 inch) was prepared and three sensors were embedded inside. One sensor was positioned in the center of the bondline and the other two sensors were located near the edge of the bondlines as illustrated in Figure 20. After curing, the sensor on the left showed no signal due to wire connection and the right sensor was 0.25 inch from the edge. The strength of the sample was 1140 psi and the failure pattern was cohesive failure.

The impedance of both sensors was recorded and the root mean square deviation (RMSD) was chosen as the damage index, which described the averaged impedance change from the baseline or the sample before any fatigue loading.

$$RMSD = \sqrt{\frac{\sum_{i=1}^{N} [Re(Z_h(\omega_i)) - Re(Z_u(\omega_i))]^2}{\sum_{i=1}^{N} [Re(Z_h(\omega_i))]^2}}$$

The RMSD between 800kHz and 1MHz was calculated and illustrated in Figure 21. The damage index of the sensor near the edge increase dramatically after the load level of 900 psi (78% of the strength) and the damage index of the middle sensor is around 1100 psi (96% of the strength). The edge sensor can detect the global bondline failure earlier than the sensor in the middle. This is expected as the stress in the bondlines is not uniform and the stress on the edge is higher while the middle is lower. As a result, the region on the edge is prone to degradation and the sensor on the edge can pick up the degradation earlier.

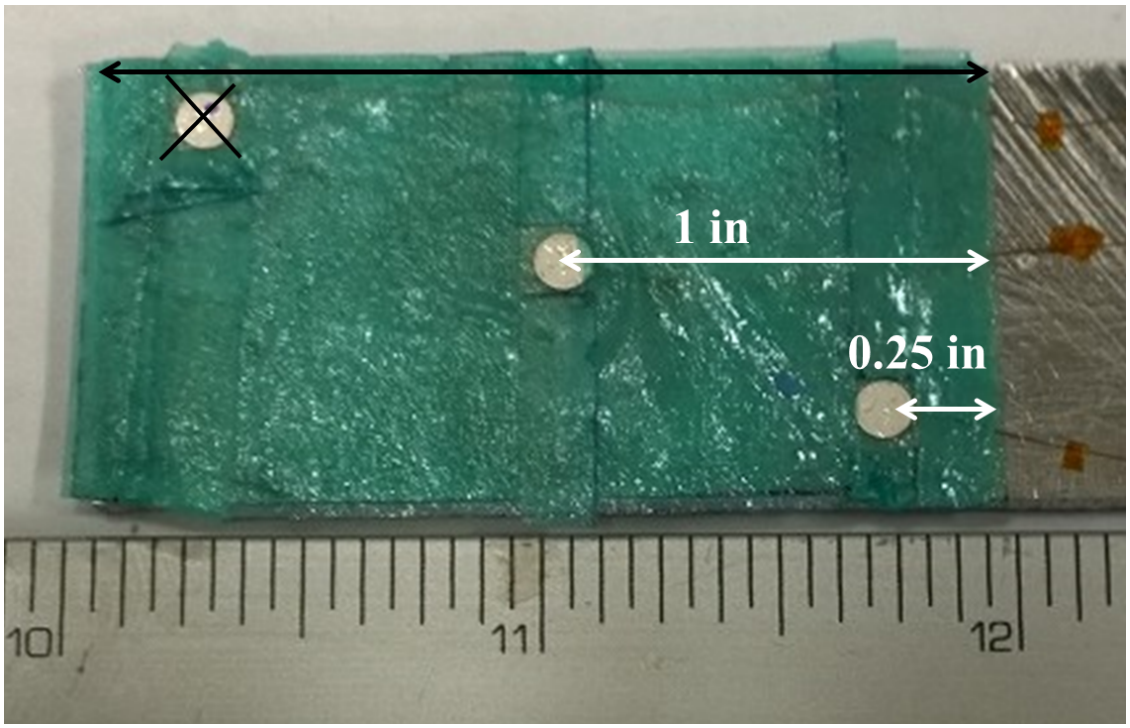

Figure 20: The adhesive bondline with two sensors embedded.

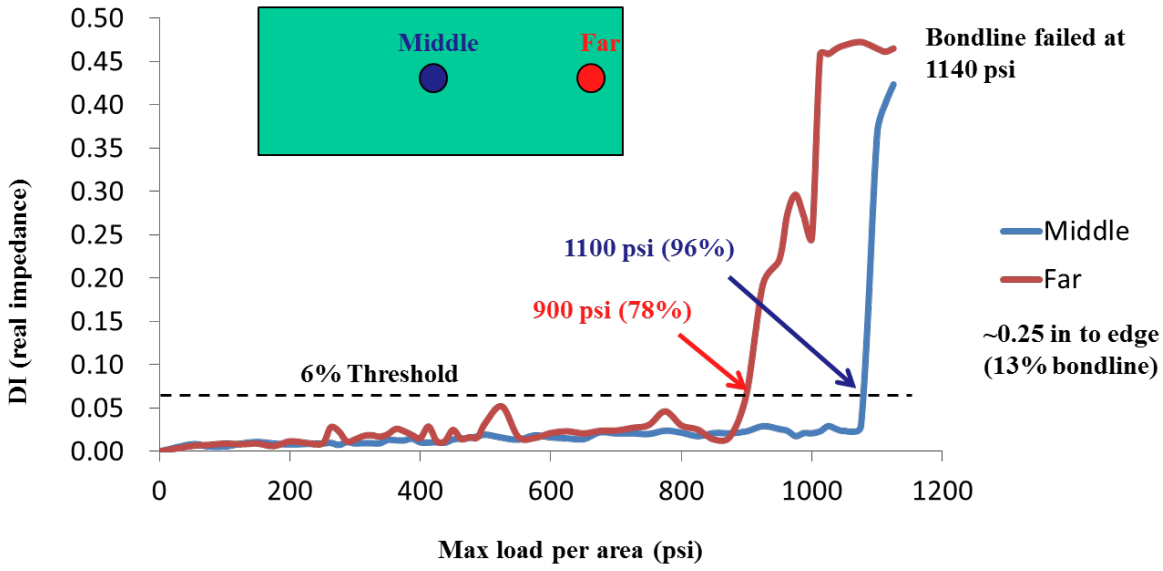

Figure 21: Damage index versus maximum load for the two embedded sensors.

Parametric Study of Sensor Performance via Finite Element Simulation

The finite element model was also developed in order to optimize the design of the piezoelectric sensor embedded in the bondline. The parametric study was conducted to understand what effect would have on the detectability.

Problem Statement

In order to be embedded into the bondline, the dimension of the piezoelectric sensor should be restricted in order to minimize the parasitic effect on the mechanical performance of the bondline. However, the piezoelectric effect will also be altered when the size of the sensor is modified. As a result, the tool would be required to study the effect of the design of the sensor on the detectability of the bondline.

Method of Approach

The finite element model has been developed to simulate the impedance behavior of the embedded sensors in the bondlines. Compared to the SEM, which was originally designed to simulate the wave propagation in the structure, the FEM provided a faster and more accurate result of the impedance of the large frequency bandwidth using the techniques of direct steady-state linear dynamic analysis. The element of C3D8E was used for the piezo-electric element and the mesh had a typical mesh dimension of 100 um to capture all the motion and deformation of the sensor.

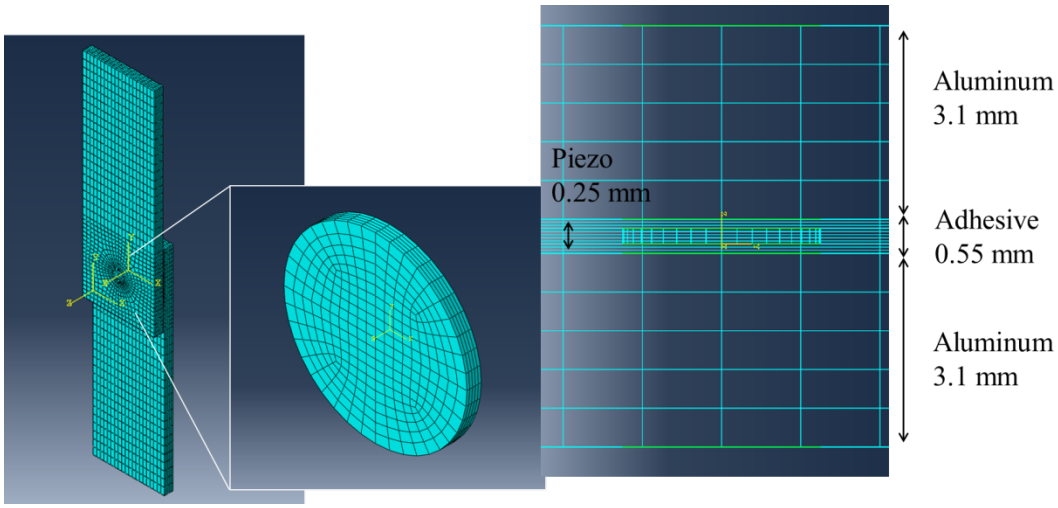

Figure 22: The FEM mesh.

The material property is shown in the following tables.

Table 8: Material properties used in the numerical simulations.

Table C.1: Mechanical properties

Property	Unit	Aluminum Al 2024-T3	CFRP T800S/3900-2	Adhesive Hysol®EA 9696	Piezo PZT-5A
E_{11}	GPa	69.00	156.00	2.60	60.97
E_{22}	GPa	69.00	9.09	2.60	60.97
E_{33}	GPa	69.00	9.09	2.60	53.19
G_{23}	GPa	25.94	3.24	1.00	21.05
G_{31}	GPa	25.94	6.96	1.00	21.05
G_{12}	GPa	25.94	6.96	1.00	22.57
ν_{23}		0.33	0.400	0.30	0.4402
ν_{13}		0.33	0.228	0.30	0.4402
ν_{12}		0.33	0.228	0.30	0.3500
ρ	kg m^{-3}	2700	1540	1100	7750

$$\mathbf{d} = \begin{bmatrix} 0 & 0 & 0 & 0 & 584 & 0 \\ 0 & 0 & 0 & 584 & 0 & 0 \\ -171 & -171 & 374 & 0 & 0 & 0 \end{bmatrix} \times 10^{-12}\,\mathrm{C\,N^{-1}} \qquad \varepsilon_\sigma = \begin{bmatrix} 1730 & 0 & 0 \\ 0 & 1730 & 0 \\ 0 & 0 & 1700 \end{bmatrix} \times \varepsilon_0$$

Results

The impedance from 50 kHz to 2 MHz was determined at the interval of 5 kHz. The results of both real and imaginary impedances are illustrated in Figure 23 in blue color. The experimental results are shown in red color. Without the further calibration of the material property as well as the dimension of the bondlines, the simulation matched the experimental result to certain extent in both frequency and amplitude.

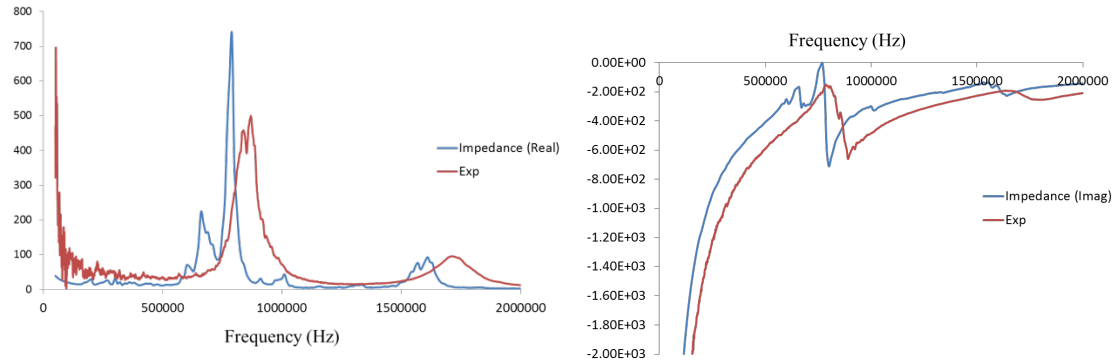

Figure 23: Comparison of numerically simulated and experimentally obtained impedance behaviour for a piezoelectric sensor embedded in the adhesive bondline.

In the literature, it was recommended that the kissing bond could be modeled by decreasing the stiffness of the interfacial element between adhesive and adherent [2,3]. The typical thickness of the element is 10 um. The stiffness of the interfacial element is tuned to different level to simulate the severity of the bondline degradation due to kissing bond as shown in Figure 24.

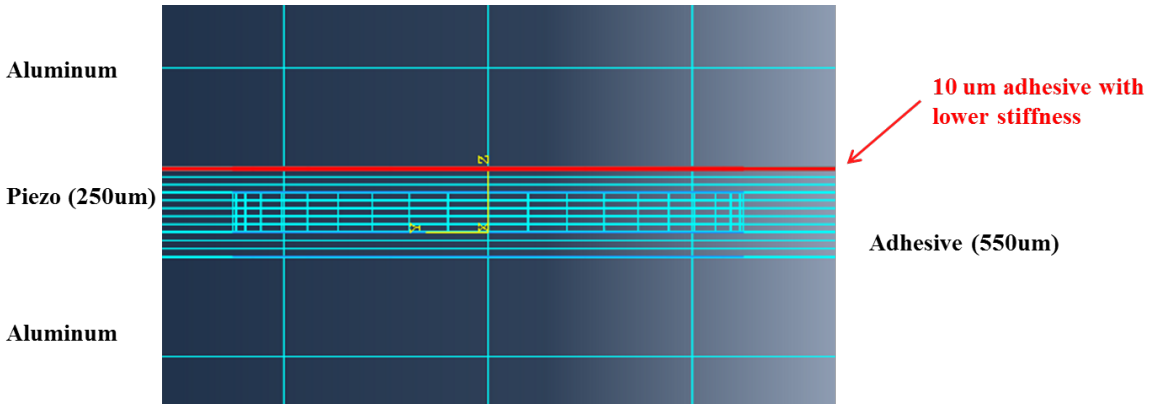

Figure 24: Kissing bond simulation is achieved via the reduction of the stiffness of the interfacial elements.

The stiffness was lowered from 10 % to 99 % and the result of simulation was plotted in Figure 25. With the decrease of the stiffness, the peak of impedance first decreases in the amplitude. After certain level, the peak of impedance starts to increase while the frequency of the peak decreases. The similar trend was observed experimentally when the load level of the sample increased and the damage level of the bondline became more severe as shown in Figure 26.

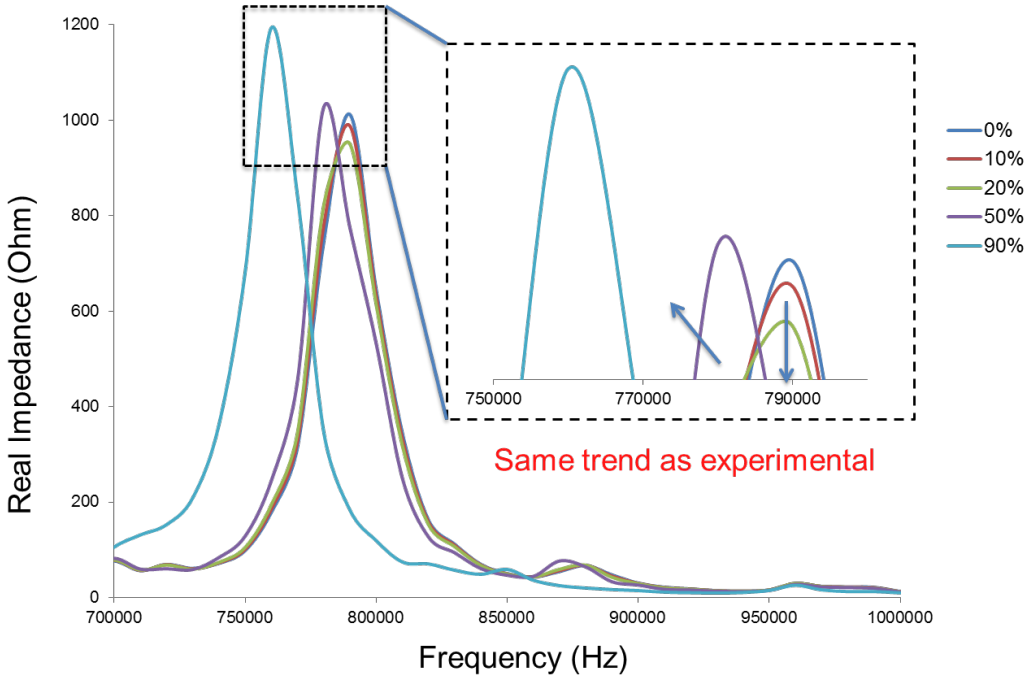

Figure 25: Numerical results for the simulation of the bondline integrity degradation due kissing bond.

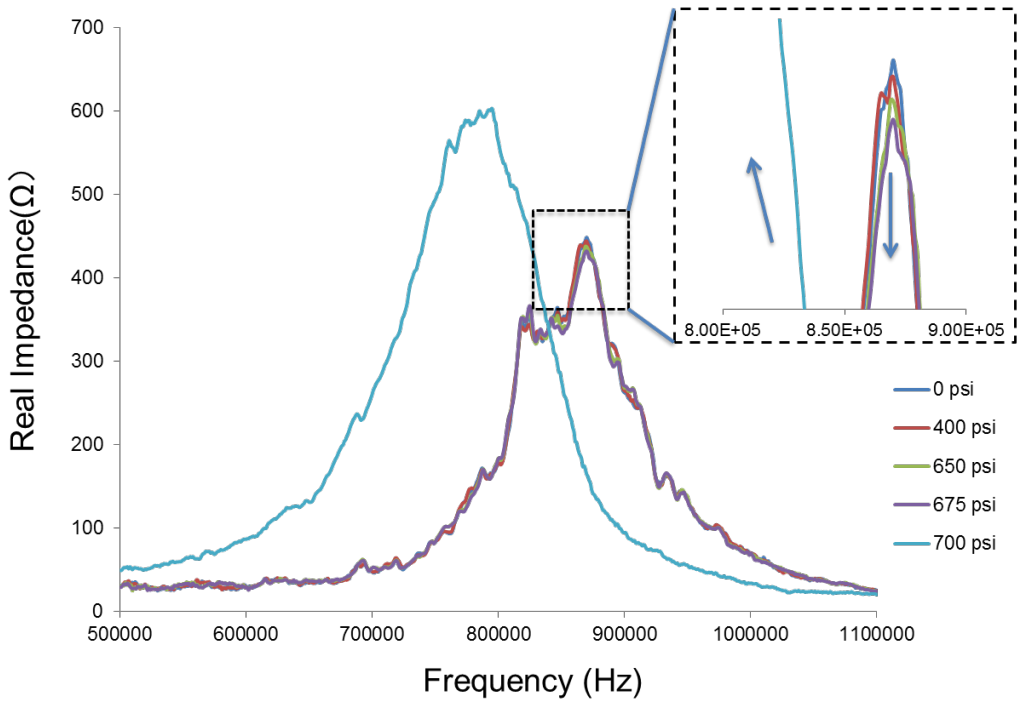

Figure 26: Experimental results of impedance show the similar trend as the simulation result

There were three parameters that were studied to evaluate sensor's performance, i.e. the diameter and the thickness of the disc-shape piezoelectric sensor embedded in the bondline as well as the distance to the damage, via the finite element simulation. As described in the previous section, the stiffness of the interfacial elements between adhesive and adherent were decreased in order to simulation the bondline degradation. For each designs of the sensor, three levels of stiffness degradation, nominal (0% of loss), degraded (10% of loss) and weak (50% of loss), were investigated. The impedance was simulated within a range from 50 kHz to 3 MHz under all the interfacial stiffness cases and the damage index was calculated from 600 kHz to 3 MHz compared to the nominal cases.

Three thicknesses of the sensor's design, 250 um, 150 um and 50 um, were investigated. The diameter of the sensor's design was fixed at 3 mm and the distance to the bondline degradation was set to 150 um. The damage index based on real impedance deviation was plotted in Figure 27. The monotonic relationship was observed between the damage index and the thickness of the sensor under both degraded and weak levels of stiffness loss. The thinner the sensor was, the higher damage index was measured under the same level of bondline degradation. It implies that the thinner design of sensor is preferred over the thick one due to the better sensitivity to the degradation.

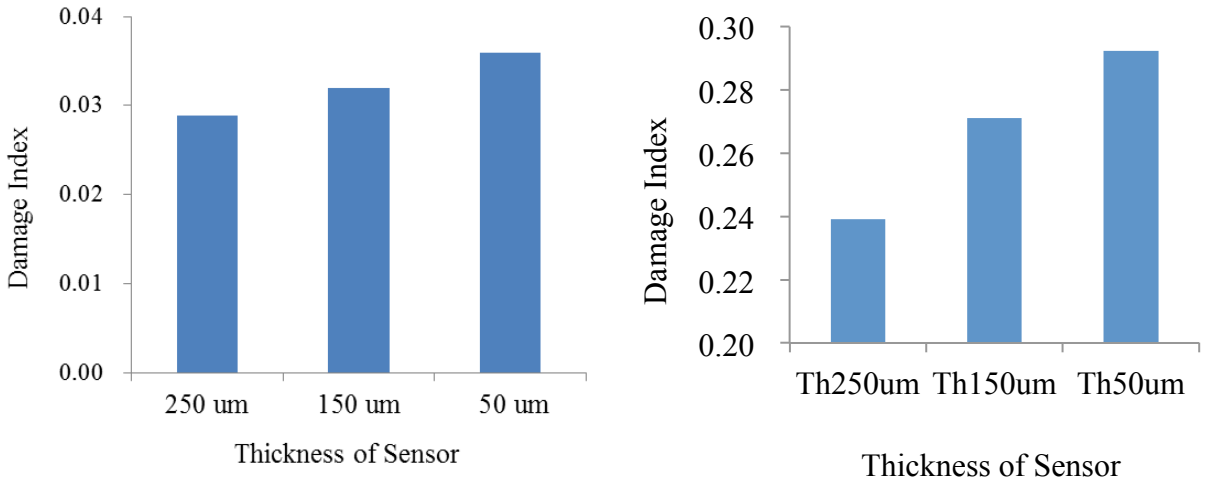

Figure 27. Shrinking down the thickness of the embedded sensor in the bondline led to increasing in the sensitivity to both left) degraded bondline property (10 % loss of interfacial element's stiffness) and right) weak bondline property (50% loss of interfacial)

Three diameters of the sensor's design, 4 mm, 3 mm and 2 mm, were investigated while the thickness of the sensors was kept at 50 um and the distance to the bondline degradation was set to 150 um. The correlation was plotted in Figure 28. Compared to the montonic dependence of thickness, shrinking down the diameter of sensors doesn't lead to a better performance. Instead, it seems that there is an optimal diameter for the embedded sensor to achieve a high sensitivity to the bondline degradation. In fact, based on the simulation, the 3 mm diameter design outperformed the 4 mm design by more than 100 % for degraded case and more than 200 % for the weak case.

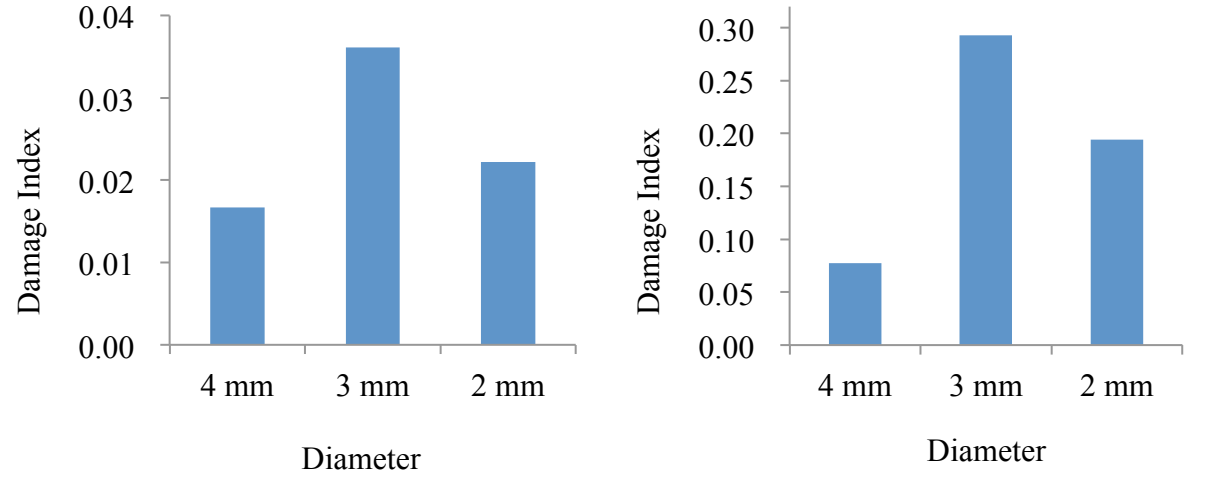

Figure 28. Shrinking down the diameter the sensors led to an increase in sensitivity first and an decrease after. 3 mm diameter design of sensor achieved the highest sensitivity to both left) degraded bondline property (10 % loss of interfacial element's stiffness) and right) weak bondline property (50% loss of interfacial element's stiffness)

The last parameter investigated is the distance from the sensor to the interfacial element of which the stiffness was decreased to simulate the bondline's degradation. The bondline thickness was kept constant while the lateral distance was adjusted to study the sensor's performance. The sensor was designed with 2 mm diameter and 50 um in thickness while the thickness of the bondline was 350 um. The distance to the interface was set to 150 um, 100 um and 50 um, which meant that the sensor was placed from the midpoint to the nearer layer to the interface. The result is plotted in Figure 29. There is no monotonic relationship between the distance and the sensor's sensitivity, which is realtively counter-intuitive. In fact, the sensitivity of the sensor was much lowered when placed around 100 um to the interface. It indicated that there is a complex interaction between the vibration on the sensor and the bondline structure. In order to find an optimal design, a thorough optimization process will be required.

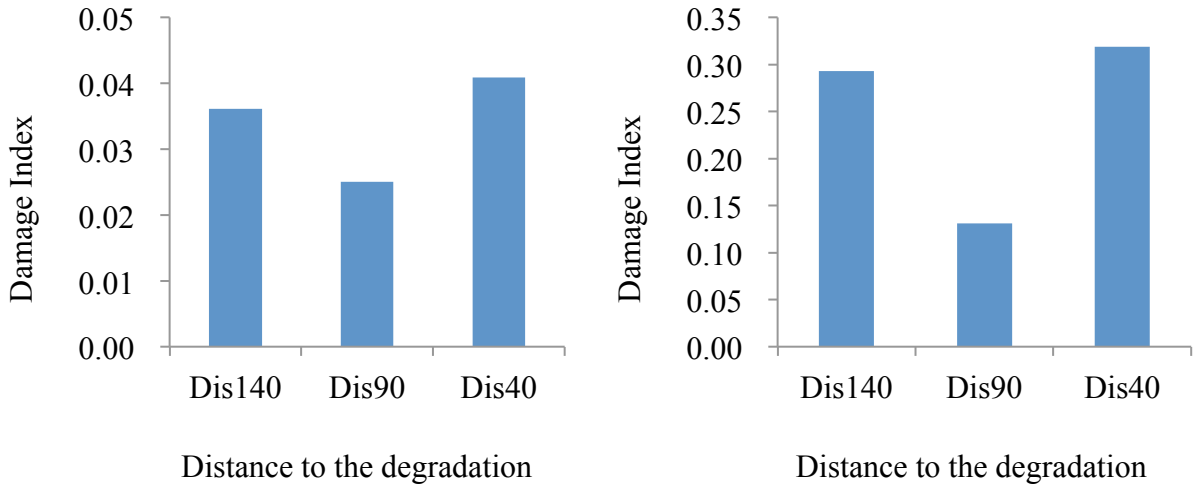

Figure 29. By placing the sensors closer to the bondline degradation, the sensitivity of the sensor was decreased first and increased after. 100 um distance result in the lowest sensitivity of the design of the sensor of 2 mm diameter and 50 um thickness to both left) degraded bondline property (10 % loss of interfacial element's stiffness) and right) weak bondline property (50% loss of interfacial element's stiffness)

Screen-printed Micro-scale Piezo-ceramics onto Polymeric Films

The works presented in the previous section showed the possibility to monitor the bondline integrity using embedded piezoelectric sensors. However, the piezoelectric sensor would require a miniaturized dimension, especially in thickness, in order to introduce minimized parasitic effect to the bondline. Traditional thin-film techniques can lead to a piezo-sensor with less than 10 um thickness, which could meet the requirements, while can only be adapted to organic piezoelectric material with much lower performance than piezoelectric ceramic material. Traditional bulk ceramic techniques can only achieve the sensor s' thickness of 200 um, which can lead to a loss of bondline strength. A novel technique of screen-printing ceramic material onto organic substrate can result in a piezoelectric sensor with the thickness of less than 10 um while maintain the same strong piezoelectric effect as conventional bulk ceramic.

This study presents the development of a process to simultaneously fabricate and deploy numerous functional, micro-scale screen-printed piezoceramics onto polymeric films and stretchable networks using nonstandard C-MOS and MEMS fabrication techniques.

Problem Statement

This study presents the development of a process to simultaneously fabricate and deploy numerous functional, micro scale screen printed piezoceramics onto polymeric films and stretchable networks using nonstandard C-MOS and MEMS fabrication techniques. Piezoceramics deployed on polymeric films or stretchable network can be embedded within structures and used to actuate ultrasonic signals or sense dynamic excitation as depicted in Figure 30.

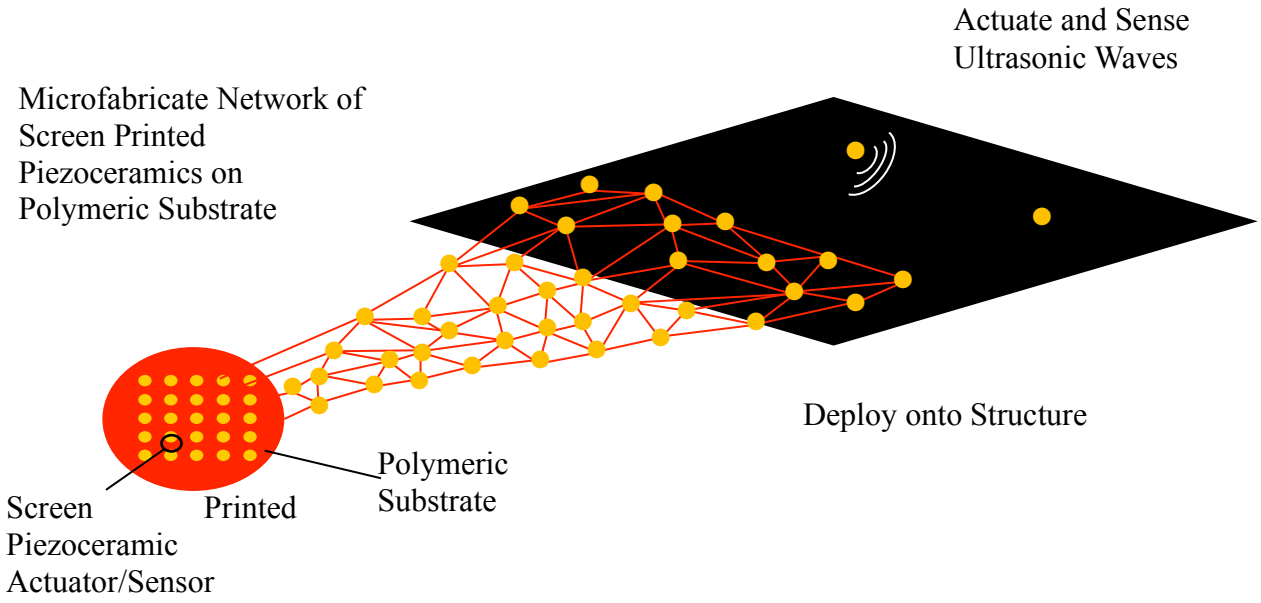

Figure 30: Schematic of proposed process including micro-fabrication of screen-printed piezoceramics on a polymeric substrate, deployment, and actuation & sensing of ultrasonic waves.

Method of Approach

The method of approach consisted of developing a novel microfabrication process to create and release complete integrated networks of numerous screen-printed piezoceramic transducers on polymeric substrates and stretchable networks. Then the networks were deployed onto structures and the functionality of the piezoceramics demonstrated.

There are multiple benefits to using the combination of microfabrication and screen printing to create the desired system, including:

- Microfabrication
  - Well suited for the simultaneous fabrication of large numbers of small devices, like billions of transistors on in a microchip.
  - Capable of creating micro-scale components.
- Screen printing
  - Capable of creating many devices simultaneously
  - Layer oriented process making it compatible with microfabrication

  - Capable of layers from 4 µm to 100 µm thick, substantially thicker than typical microfabrication.

These traits enable the mass fabrication of small-scale devices in an integrated system, on the order of 10s of microns thick. Additionally microfabricated expandable networks provide a method to deploy microfabricated devices over macro areas. Despite these benefits, processing issues complicate and have previously prevented deployment of functional screen-printed piezoceramics on polymeric films.

The following major tasks were pursued to enable mass fabrication and deployment of functional, micro scale screen-printed piezoceramics on polymeric films and stretchable networks:

- Material selection and screen printing functional piezoceramics.
- Process development
  - Development of nonstandard microfabrication processes and screen printing capabilities
  - Screen print piezoceramics on a high temperature tolerant working substrate
  - Reversal of typical fabrication order; creating the complete integrated network of devices and electronics then depositing the target polymeric substrate onto them.
  - Integration of multiple layers of chemical protection
  - Etch of entire high temperature substrate releasing the complete system onto polyimide films and stretchable networks
- Deployment & Testing

Material Selection and Screen Printing of Functional Piezoceramics

While stretchable networks and screen printed piezoceramics have been demonstrated individually, the specific processing requirements in their fabrication would drive the requirements of the remainder of the fabrication process. Therefore a polymeric substrate was selected. A specific chemistry of piezoceramic was also selected and testing performed to ensure the functionality of the screen-printed piezoceramics being developed.

Process Development

A fabrication process using a combination of nonstandard microfabrication and screen-printing techniques was developed to enable the release of screen-printed piezoceramics onto polymeric films and stretchable networks. In the process, the order of fabrication was arranged to move high temperature exposure, on the order of 1000 °C to the beginning of the overall process and delay the addition of materials that cannot withstand these temperatures as illustrated in Figure 31 and Figure 32.

This process required a reversal of typical fabrication order. Because of the nature of the process, experimentation was necessary to determine material compatibilities and develop capabilities enabling many of the less standard steps. The process integrated multiple protective layers, which had to be developed, to prevent chemical exposure of incompatible components.

In the resulting process multiple piezoceramic elements were screen printed and sintered at 1000 °C on a high temperature tolerant working substrate. All electrodes and wiring were also deposited on the high temperature working substrate creating the complete network of piezoelectric transducers. Then in a reversal of typical fabrication processing, the polymeric service substrate was deposited onto the complete system. Finally the entire high temperature working substrate was etched off releasing the entire system onto the polyimide service substrate.

Deployment and Testing

The released samples were deployed and tested to demonstrate that the piezoceramics maintained functionality and were not degraded by the processing. While the process was developed with survival of the piezoceramics in mind, it does involve some chemicals that can degrade or destroy piezoceramic materials.

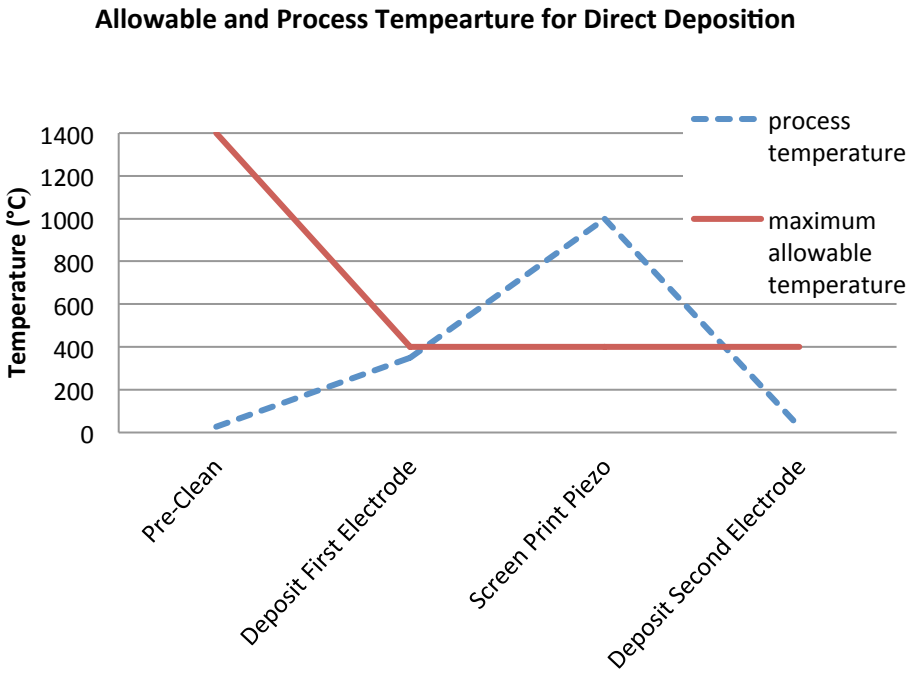

Figure 31: Processing temperature and maximum allowable temperature at key steps in direct deposition fabrication. The maximum allowable temperature is exceeded.

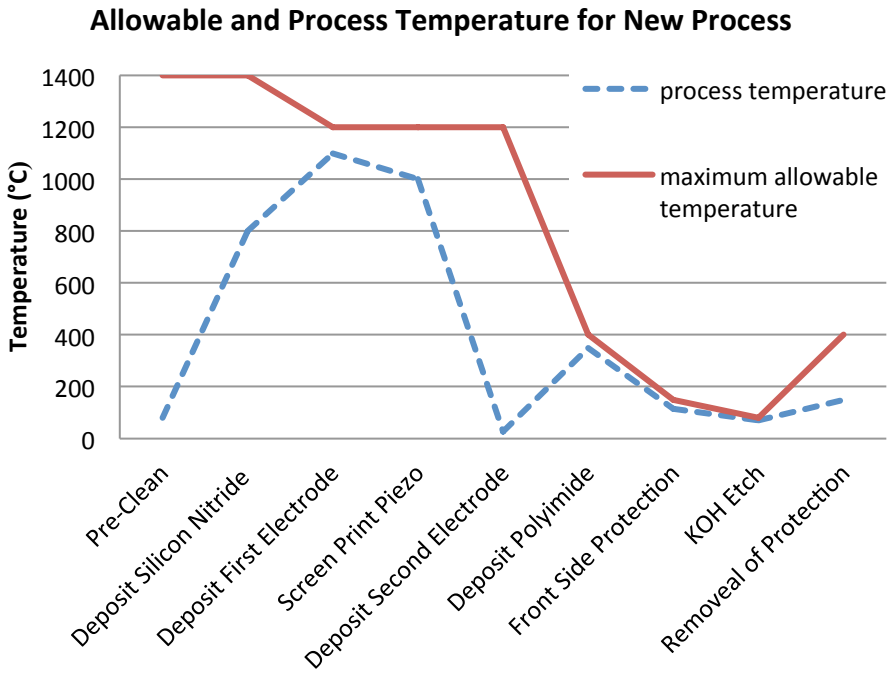

Figure 32: Processing temperature and maximum allowable temperature at key steps in the new fabrication process. The steps were re-organized so that the maximum allowable temperature is not exceeded.

Key process steps included:

- Deposit etch stop layer
- Screen print and sintering piezoceramics
- Evaporation coat metallic electronics and wiring
- Spin coat polymer substrate
- Pattern and etching stretchable network pattern
- Release network from rigid working substrate
- Deploying network

Results

Lead Zirconate Titanate (PZT) based piezo-ceramics have been successfully printed, deployed, and tested on polymeric substrates and stretchable networks. These piezoceramics had a thickness of 30 µm, with an overall network thickness including all wiring, electrodes and a polyimide carrier layer peaking at 53 µm. Interconnecting regions were 12 µm thick. This is small enough to be embedded between laminates in a composite structure or completely within adhesive layers without structural modification.

Pitch catch signal propagation testing, similar to signals used in SHM, sample did not indicate any significant degradation to the piezoceramics due to processing when compared to a baseline that had not undergone the release process. This can be seen in Figure 33, which shows the peak

voltage of signals measured in a baseline and a released sample. In these tests a Gaussian windowed 5 peak tone burst at the designated frequency with a peak input voltage of 30 V was actuated by one screen printed piezoceramic, propagating 14 mm through 0.5 mm thick silicon and received by another screen printed piezoceramic. Similar results were found for signal energy of the first wave packet to arrive and total signal energy. Impact detection capabilities were also tested on the stretched sample, which showed that the entire network survived fabrication, release, and stretch.

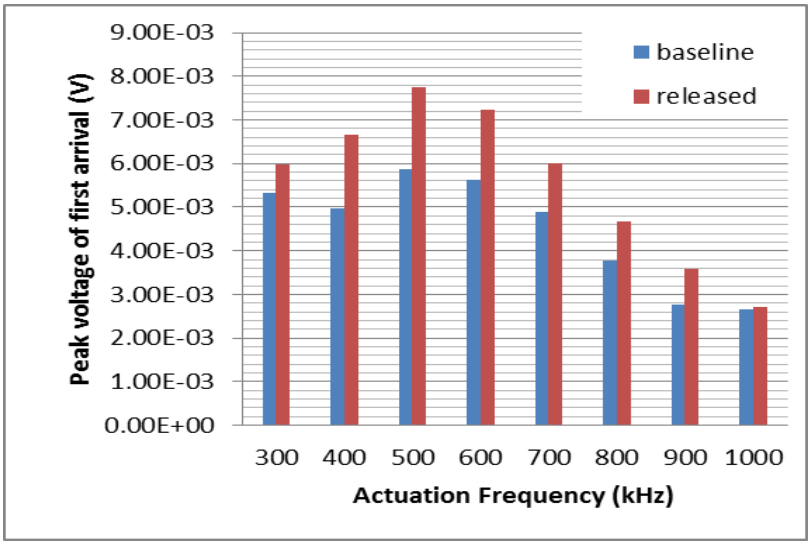

Figure 33: Peak voltage of first signal arrival in baseline and released samples. Piezos were 2 mm in radius by 30 μm thick and 14 mm apart on center mounted on 0.5 mm thick silicon and actuated with 30 V Gaussian windowed inputs.

Release of Screen Printed Piezo-ceramics onto a Polyimide Substrate

Screen-printing was selected as a method of producing micro-scale piezoelectric elements in a layer oriented micro-fabrication compatible process. Screen-printing is capable of producing arrays of numerous elements simultaneously, with smaller sizes then are possible using bulk ceramic processing techniques. However, once printed the piezoceramics require sintering at temperatures greater than 1000°C. Additionally, screen-printed piezoceramics bond onto the substrate they are printed on. This has severely limited application because few materials can survive such extreme temperatures.

Problem Statement

Develop designs and processes to mass fabricate and deploy high efficiency piezoceramic actuator/sensors on a micro fabricated thin film organic substrate and test-released specimens.

Method of Approach

The approach to this is to screen print and sinter the screen-printed piezoceramics on a high temperature processing substrate and then release them onto an organic service substrate. This

requires modified, reversed fabrication methods to create the entire system of screen printed piezoceramics, electrodes, and wiring on the processing substrate, and then deposit the service substrate onto the devices and release the complete system.

Results

Lead Zirconate Titanate (PZT) based piezo-ceramics have been successfully printed, deployed, and tested on organic substrates and stretchable networks as shown in Figure 34. These piezoceramics had a thickness of 30 µm, with an overall network thickness including all wiring, electrodes and a polyimide carrier layer peaking at 53 µm. Interconnecting regions were 12 µm thick. This is small enough to be embedded between laminates in a composite structure or completely within adhesive layers without structural modification.

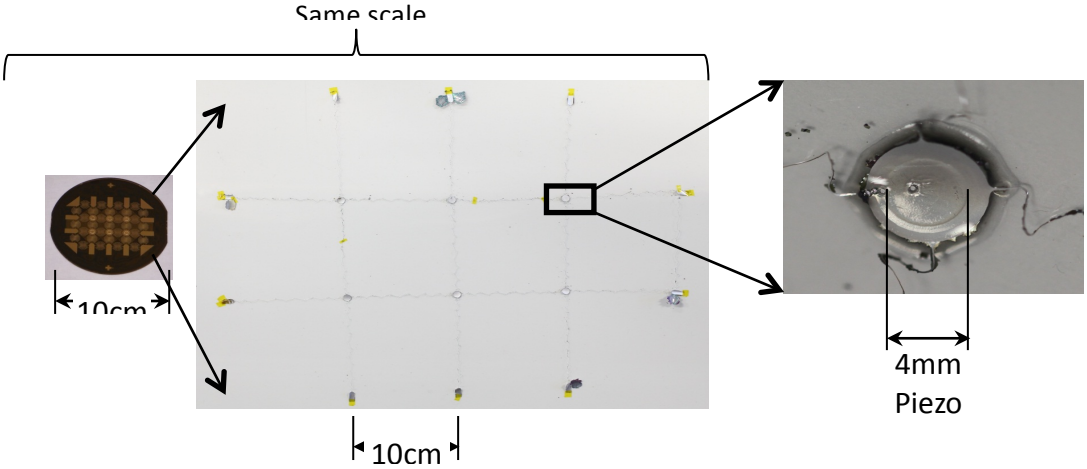

Figure 34: Functional screen-printed piezoceramics deployed on a stretchable network.

Pitch catch signal propagation testing, similar to signals used in SHM, sample did not indicate any significant degradation to the piezoceramics due to processing when compared to a baseline that had not undergone the release process. In these tests a Gaussian windowed 5 peak tone burst at the designated frequency with a peak input voltage of 30 V was actuated by one screen printed piezoceramic, propagating 14 mm through 0.5 mm thick silicon and received by another screen printed piezoceramic. Similar results were found for signal energy of the first wave packet to arrive and total signal energy. Impact detection capabilities were also tested on the stretched sample, which showed that the entire network survived fabrication, release, and stretch. In addition, multi-functional sensor systems have been created on polyimide substrates, with screen-printed piezoceramics on one side and a network of resistive temperature detectors (RTDs) opposite them as can be seen in **Error! Reference source not found.**.

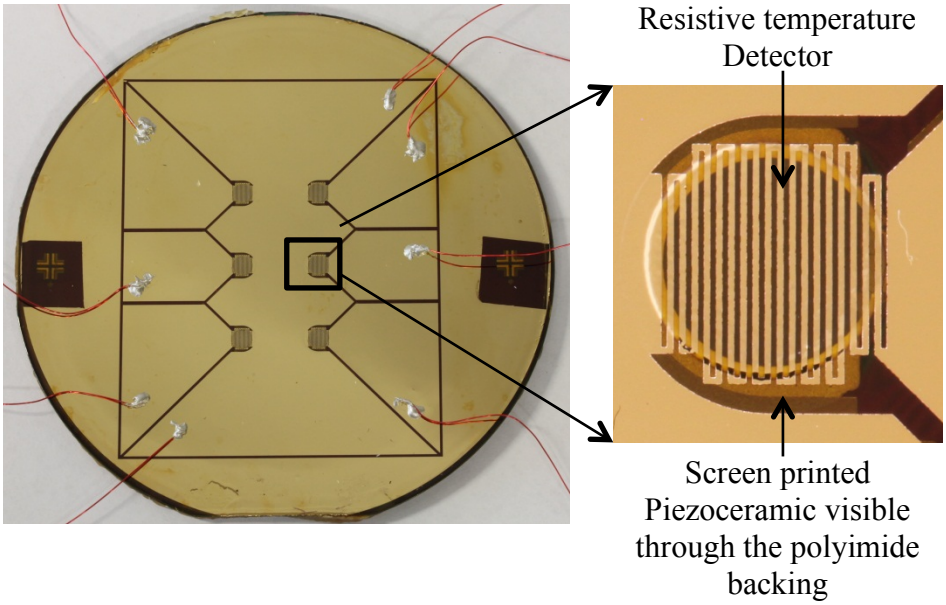

Figure 35: Functional RTDs and screen-printed piezoceramics on the same backing.

Preliminary experimental investigations regarding the challenging task of embedding miniaturized single sensors inside the adhesive layer have been conducted in the Structures and Composites Laboratory at Stanford University (Figure 36). The aim of these experiments was to assess the feasibility of the proposed approach with respect to its effectiveness in bondline integrity monitoring. Initial results confirmed the feasibility of the proposed approach in detecting bondline integrity degradation and indicating the existence of kissing bonds.

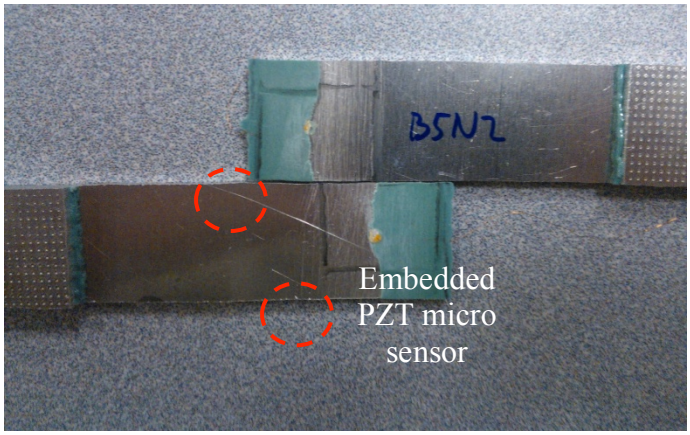

Figure 36: Interfaces of adhesively bonded aluminum joint with embedded active PZT micro sensor.

A novel design of the screen-printed piezoelectric sensors was achieved that enables their successful embedding into the adhesive bondlines. With the elimination of the stretchable wires as in the previous design, 55 screen-printed sensors were simultaneously fabricated on a single 4-

inch wafer, compared to 6 sensors of the previous design. The piezoelectric sensors have a range of different diameters from 0.75 mm to 3 mm in order to investigate the optimal dimensions with respect to their actuation and sensing effectiveness, as well as to the introduced parasitic effects on the bondlines. The piezoelectric sensors sit on a node of 5 mm x 5 mm which serves as the signal and ground electrodes for wire connection.

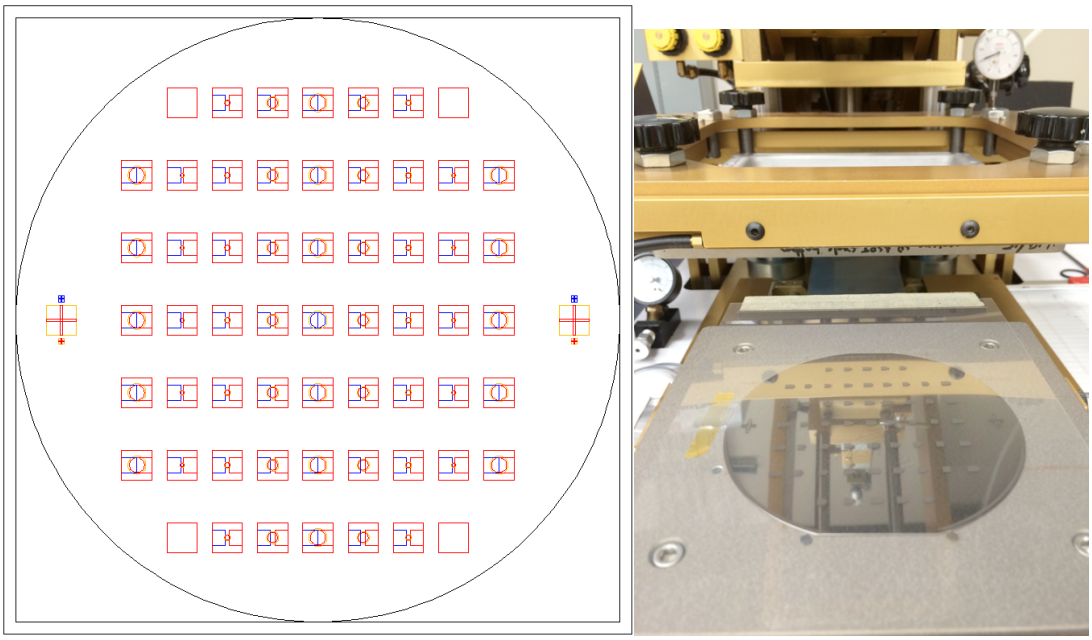

Figure 37: The new design of the screen-printed piezoelectric sensors. Fifty five sensors can be fabricated on a single 4-inch wafer.

1.4 CONCLUSION

Compared to conventional bolted joints, bonded joints have superior mechanical properties in terms of light weight, less stress concentration, etc. However, due to the lack of confidence on the bondline integrity level during fabrication and service, the large adaption of bonded joints onto airplane primary structural components is restricted by regulations and standards. Among all the defects that can be found in adhesive bondlines, one type of interfacial weakness, the kissing bond, is the most challenging one. This is due to the catastrophic failure it can cause to the bondline as well as to the almost impossible early detection using conventional non-destructive evaluation (NDE) or structural health monitoring (SHM) techniques.

We developed and tested a break-through technique to monitor the bondline integrity by embedding piezoelectric sensors into the bonded joints. The impedance-based detection algorithms were used by measuring the electromechanical impedance of the embedded sensors. Since the sensors are positioned in the bondlines, close to the interface of adhesive and adherent, where the kissing bond could occur, any small change in the interface would affect the EMI response of the sensor. The EMI behavior of the embedded sensor under static loading was studied. The single lap joints with sensor embedded inside were exposed to an incremental

tensile load. The impedance was recorded under zero load condition before a higher load was exerted on the sample. Across all the tested samples, a similar behavior was observed, i.e. the impedance of the sensor is kept constant until a certain load level, after which, the impedance changes dramatically from the pristine state. The root mean square deviation was defined as the damage index to quantify the change of impedance.

A finite element model was also developed to investigate the impedance behavior of the embedded piezo sensor. In order to simulate the behavior of kissing bond, the stiffness of the interface elements of the adhesive was degraded. The degradation of this 10 um thick element would not affect the global stiffness of the lap joint. However, it would affect the impedance behavior of the embedded sensors significantly. Preliminary simulation results matched with the experimental result qualitatively and similar trend of the decrease of resonant frequency was seen when the sample was prone to failure. More samples were tested after and the model was developed to describe the correlation between the static load and the damage index. The model would provide a baseline to predict the strength of the bondline, before the failure of the sample. One sample with unknown surface preparation was fabricated and tested to verify the model. The prediction converged at around 60% of the maximum external load and was off by less than 10% from the actual strength.

In order to design and fabricate the piezoelectric sensor to be embedded into the bondlines, a simulation model was developed to understand the effect of different design parameters like sensor size and thickness on the performance. Besides that, a novel method was required to fabricate a piezoelectric sensor with both miniaturized size and strong piezoelectric characteristics .Currently, the fundaments of screen printing techniques for ceramic piezoelectric material onto organic substrate has been developed. However, the extensive work is needed to optimize the release process in order to yield a comparable performance as the bulk ceramics. It would be the last missing piece to monitor the bondline integrity via the adhesive with built-in sensors.

1.5 PUBLICATIONS

1. Zhuang, Yitao; Kopsaftopoulos, Fotis; Chang Fu-Kuo; "**Bondline Integrity Monitoring of Adhesively Bonded Structures via an Electromechanical Impedance Based Approach**", accepted paper in the *6th World Conference on Structural Control and Monitoring (6WCSCM)*, July 15-17, 2014, Barcelona, Spain.
2. Salowitz, Nathan; Guo, Zhiqiang; Roy, Surajit; Nardari, Raphael; Li, Yu-Hung; Kim, Sang-Jong; Kopsaftopoulos, Fotis; Chang, Fu-Kuo; "**A vision on stretchable bio-inspired networks for intelligent structures**", Invited Keynote Paper, Structural Health Monitoring 2013.
3. K. Lonkar, "**Modeling of Piezo-Induced Ultrasonic Wave Propagation for Structural Health Monitoring**," *PhD Thesis, Stanford University, CA, USA, 2013*.
4. Salowitz N., Guo Z., Roy S., Nardari R., Li Y.-H., Kim S.-J., Kopsaftopoulos F., Chang F.-K., "**Recent advancements and vision toward stretchable bio-inspired networks for intelligent structures**", Structural Health Monitoring, Vol. 13, No. 6, pp. 609–620, 2014.
5. Dugnani R., Zhuang Y., Kopsaftopoulos F.P., Chang F.-K., "**Adhesive Bond-line Degradation Detection via a Cross-correlation Electro Mechanical Impedance-based Approach**", accepted, International Journal of Structural Health Monitoring
6. Zhuang Y., Kopsaftopoulos F.P., Chang F.-K., "**Bondline integrity monitoring of adhesively bonded structures via an electromechanical impedance based approach**", accepted, Proceedings of the 10th International Workshop on Structural Health Monitoring (IWSHM), Stanford University, USA, September 2015.
7. Zhuang Y., Li Y.-H., Kopsaftopoulos F.P., Chang F.-K., "**A self-diagnostic adhesive for monitoring bonded joints in aerospace structures**", Proceedings of the SPIE 9803, Sensors and Smart Structures Technologies for Civil, Mechanical, and Aerospace Systems 2016, 98030I, April 2016.http://dx.doi.org/10.1117/12.2219361
8. Zhuang Y., Kopsaftopoulos F.P., Chang F.-K., "**A self-diagnostic adhesive for monitoring bonded joints in composite structures**", Proceedings of the Composites and Advanced Materials Expo (CAMX), Dallas, TX, USA, October 2015.

1.6 REFERENCES

1. Achenbach, J.D., & Parikh, O.K. "Ultrasonic Analysis of Nonlinear Response and Strength of Adhesive Bonds." *J. Adhes. Sci.* 5(8) (1991): 601-608
2. Baltazar, A., Rokhlin, S.I., & Pecorari, C. "The Relationship between Ultrasonic and Micromechanical Properties of Contacting Rough Surfaces" *J. Mech. Phys. Solids* 50(2002): 1397-1416
3. Baltazar, A., Wang, L., Xie, B, & Rokhlin, S.I. "Inverse Ultrasonic Determination of Imperfect Interfaces and Bulk Properties of A Layer between Two Solids." *Acoustical Society of America.* 114 (3)(2003): 1424-1434
4. Brotherbood, C.J., Drinkwater, B.W., & Dixon, S. "The Detectability of Kissing Bonds in Adhesive Joints Using Ultrasonic Techniques." *Ultrasonic* 41(7) (2003): 521-529
5. Ehehart, B., Valeskes, B., Muller, C.E., Bockenheimer, C. "Methods for the Quality Assessment of Adhesive Bonded CFRP Structures -A Resumé." *2nd International Symposium on NDT*, Aerospace 2010, We.5.B.2
6. Ihn, J.B., & Chang, F.K. "Built-in Diagnostics for Monitoring Crack Growth in Aircraft Structures" *Proceedings of the 3rd international Workshop on Structural Health Monitoring*. Stanford, CA, Sept 2001 pp. 284-295
7. Ihn, J.B., & Chang, F.K. "Hot Spot Monitoring for Aircraft Structures", *Advanced Smart Materials and Smart Structures Technology*. 2004
8. Ihn, J.B., & Chang, F.K. "Detection and Monitoring of Hidden Fatigue Crack Growth Using a Built-in Piezoelectric Sensor/actuator Network." *Smart Material Structure* 13(2004): 609-620
9. Jiao, D., & Rose, J.L. "An Ultrasonic Interface Layer Model for Bond Evaluation." *J. Adhesion Science and Technology* 5(8) (1991): 631-646
10. Light, G.M., & Kwun, H. "Nondestructive Evaluation of Adhesive Bond Quality, State-of-the-Art Review." *NTIAC* 89(1) (1989)
11. Maeva, E., Severina, I., Bondarenko, S., Chapman, G., O'Neil, B., Severin, F., & Maev, R. Gr. "Acoustical methods for the investigation of adhesively bonded structures: A review." *Can. J. Phys.* 82(2004): 981-1025
12. Margetan, F.J., Thompson, R.B., & Gray, T.A. "Interfacial Spring Model for Ultrasonic Interactions with Imperfect Interfaces: Theory of Oblique Incidence and Application to Diffusion-Bonded Butt Joints." *Journal of Nondestructive Evaluation*. 7 (3-4) (1988)
13. Nagy, P.B. "Ultrasonic Classification of Imperfect Interfaces." *J. Adhesion Science and Technology* 5(1991): 619-630
14. Rokhlin, S.I., Wang, L., Xie, B., Yakovlev, V.A. & Adler, L. "Modulated Angle Beam Ultrasonic Spectroscopy for Evaluation of Imperfect Interfaces and Adhesive Bonds." *Ultrasonic* 42 (2004): 1037-1047.
15. Rokhlin, S.I., Xie, B, & Baltazar, A. "Quantitative Ultrasonic Characterization of Environmental Degradation of Adhesive Bonds." *J. Adhesion Sci. Technol.* 18(3)(2004): 327-359
16. Tang, Z., Cheng, A., & Achenbach, J.D. "An Ultrasonic Technique to Detect Nonlinear Behaviour Related to Degradation of Adhesive Joints." *QNDE*, D.O. Thompson, D.E. Chimenti (Eds), Vol. 17, Plenum Press, New York, 1998.
17. Wang, N., Lobkis, O. I., Rokhlin, S. I., & Cantrell, J. H. "Ultrasonic Characterization of Interfaces in Composite Bonds." *AIP Conf. Proc.* 1335, 1079 (2011)

AFOSR Deliverables Submission Survey

Response ID:7031 Data

1.

Report Type

Final Report

Primary Contact Email

Contact email if there is a problem with the report.

fkchang@stanford.edu

Primary Contact Phone Number

Contact phone number if there is a problem with the report

(650) 723-3466

Organization / Institution name

Stanford University

Grant/Contract Title

The full title of the funded effort.

Self-Diagnostic Adhesive for Bonded Joints in Aircraft Structures

Grant/Contract Number

AFOSR assigned control number. It must begin with "FA9550" or "F49620" or "FA2386".

FA9550-13-1-0139

Principal Investigator Name

The full name of the principal investigator on the grant or contract.

Fu-Kuo Chang

Program Officer

The AFOSR Program Officer currently assigned to the award

B. L. ("Les") Lee

Reporting Period Start Date

03/15/2013

Reporting Period End Date

03/14/2016

Abstract

Bondline integrity is one of the most critical concerns in the design and operation of aircraft and spacecraft structures up to date. Nevertheless, current state-of-the-art non-destructive evaluation (NDE) and structural health monitoring (SHM) techniques are incapable of offering mature solutions regarding bondline integrity monitoring. Therefore, the objective of the proposed research is the development of a complete approach for integrity monitoring and self-diagnosis of adhesively bonded structures. During the reporting period, three major accomplishments were achieved:
1) Screen-printed piezo-electric sensors of the new design were developed and fabricated. The new sensors had a smaller dimension compared to the previous design to minimize the parasitic effect when embedded into bondlines. 2) The developed impedance-based diagnostic algorithms were validated under the fatigue/dynamic loading condition. 3) Both SEM (Spectral Element Modeling) and FEM (Finite Element Modeling) simulation of the impedance of the embedded piezo-elelctric sensor was conducted.

Distribution Statement

This is block 12 on the SF298 form.

Distribution A - Approved for Public Release

Explanation for Distribution Statement

If this is not approved for public release, please provide a short explanation. E.g., contains proprietary information.

SF298 Form

Please attach your SF298 form. A blank SF298 can be found here. Please do not password protect or secure the PDF The maximum file size for an SF298 is 50MB.

AFD-070820-035_filled.pdf

Upload the Report Document. File must be a PDF. Please do not password protect or secure the PDF . The maximum file size for the Report Document is 50MB.

AFOSR final Report_v3.pdf

Upload a Report Document, if any. The maximum file size for the Report Document is 50MB.

Archival Publications (published) during reporting period:

1. Zhuang, Yitao, Kopsaftopoulos, Fotis, Chang Fu-Kuo, "Bondline Integrity Monitoring of Adhesively Bonded Structures via an Electromechanical Impedance Based Approach", accepted paper in the 6th World Conference on Structural Control and Monitoring (6WCSCM), July 15-17, 2014, Barcelona, Spain.

2. Salowitz, Nathan, Guo, Zhiqiang, Roy, Surajit, Nardari, Raphael, Li, Yu-Hung, Kim, Sang-Jong, Kopsaftopoulos, Fotis, Chang, Fu-Kuo, "A vision on stretchable bio-inspired networks for intelligent structures", Invited Keynote Paper, Structural Health Monitoring 2013.

3. K. Lonkar, "Modeling of Piezo-Induced Ultrasonic Wave Propagation for Structural Health Monitoring," PhD Thesis, Stanford University, CA, USA, 2013.

4. Salowitz N., Guo Z., Roy S., Nardari R., Li Y.-H., Kim S.-J., Kopsaftopoulos F., Chang F.-K., "Recent advancements and vision toward stretchable bio-inspired networks for intelligent structures", Structural Health Monitoring, Vol. 13, No. 6, pp. 609–620, 2014.

5. Dugnani R., Zhuang Y., Kopsaftopoulos F.P., Chang F.-K., "Adhesive Bond-line Degradation Detection via a Cross-correlation Electro Mechanical Impedance-based Approach", accepted, International Journal of Structural Health Monitoring

6. Zhuang Y., Kopsaftopoulos F.P., Chang F.-K., "Bondline integrity monitoring of adhesively bonded structures via an electromechanical impedance based approach", accepted, Proceedings of the 10th International Workshop on Structural Health Monitoring (IWSHM), Stanford University, USA, September 2015.

7. Zhuang Y., Li Y.-H., Kopsaftopoulos F.P., Chang F.-K., "A self-diagnostic adhesive for monitoring bonded joints in aerospace structures", Proceedings of the SPIE 9803, Sensors and Smart Structures Technologies for Civil, Mechanical, and Aerospace Systems 2016, 98030I, April 2016. http://dx.doi.org/10.1117/12.2219361

8. Zhuang Y., Kopsaftopoulos F.P., Chang F.-K., "A self-diagnostic adhesive for monitoring bonded joints in composite structures", Proceedings of the Composites and Advanced Materials Expo (CAMX), Dallas, TX, USA, October 2015.

New discoveries, inventions, or patent disclosures:

Do you have any discoveries, inventions, or patent disclosures to report for this period?

No

Please describe and include any notable dates

Do you plan to pursue a claim for personal or organizational intellectual property?

Changes in research objectives (if any):

Change in AFOSR Program Officer, if any:

Extensions granted or milestones slipped, if any:

AFOSR LRIR Number

LRIR Title

Reporting Period

Laboratory Task Manager

Program Officer

Research Objectives

Technical Summary

Funding Summary by Cost Category (by FY, $K)

	Starting FY	FY+1	FY+2
Salary			
Equipment/Facilities			
Supplies			
Total			

Report Document

Report Document - Text Analysis

Report Document - Text Analysis

Appendix Documents

2. Thank You

E-mail user

Sep 30, 2016 14:45:50 Success: Email Sent to: fkchang@stanford.edu